Toxoplasma ferlin1 is a versatile and dynamic mediator of microneme trafficking and secretion

Daniel N.A. Tagoe[1], Allison A. Drozda[1], Isabelle Coppens[2], Bradley I. Coleman[1†], Marc-Jan Gubbels[1§]

[1]Biology Department of Biology, Boston College, Chestnut Hill, MA 02467, USA

[2]Department of Molecular Microbiology and Immunology, Johns Hopkins University Bloomberg School of Public Health, Baltimore, Maryland, USA

[§]Correspondence to Marc-Jan Gubbels, gubbelsj@bc.edu

[†]Present address: Bradley. I Coleman, Harvard Medical School, Boston, Massachusetts, USA

Running title: *Toxoplasma* ferlin 1 acts on micronemes

Abstract

Calcium-dependent exocytosis of the microneme organelles that facilitate host cell invasion is critical for obligate intracellular apicomplexan parasites such as *Toxoplasma gondii*. Ferlins represent a protein family with roles in exocytosis containing multiple Ca^{2+}-sensing C2 domains. Here we defined the role of *T. gondii*'s ferlin 1 (FER1) in microneme biology. FER1 localized dynamically to several compartments of the parasite's secretory pathway as well as to an apical spot near the site of microneme secretion. FER1 function was dissected by overexpression of a variety of N-terminally tagged alleles causing dominant negative phenotypes. This demonstrated FER1 traffics microneme organelles at several discrete steps of their natural trajectories: 1. from ELC to the subpellicular microtubules; 2. along the subpellicular microtubules to the apical end; 3. into the conoid; 4. and inferred from observed retrograde transport from the subpellicular microtubules, recycling of micronemes from mother to daughter parasites. Furthermore, full-length FER1 overexpression results in a squirt of microneme release sufficient for host cell egress. This indicates FER1 facilitates fusion of the most apical, radially organized micronemes with the plasma membrane. Moreover, FER1 acts differentially on the Rab5A/C-dependent and -independent microneme sub-populations. Finally, apical FER1 overlaps with the presence of VP1, a pyrophosphatase proton pump. Integrating all new insights, we propose a model of microneme exocytosis wherein the radial micronemes constitute a readily releasable vesicle pool primed by acidification.

Keywords: exocytosis/calcium/ferlin/microneme/trafficking/*Toxoplasma*

42 **Introduction**

43 In humans, the apicomplexan parasite *Toxoplasma gondii* causes birth defects, vision
44 loss, myocarditis and encephalitis. Lytic replication cycles unfolding through repetitive rounds of
45 host cell invasion, intracellular replication and host cell egress are central to the pathogenesis of
46 toxoplasmosis [1]. The micronemes in apicomplexan parasites are pivotal for successful host cell
47 invasion as they contain adhesion molecules facilitating gliding motility and host cell association
48 [2, 3]. In addition, the *Toxoplasma gondii* micronemes encode a pore-forming protein, PLP1, that
49 permeabilizes both the parasitophorous vacuole and host plasma membrane, which is required
50 for efficient host cell egress [4, 5]. The parasite's signal transduction pathways controlling the
51 correct timing of micronemes secretion comprises cGMP, Ca^{2+} and phosphatidic acid (PA) [6],
52 accompanied by a crucial cAMP-mediated switch between the intracellular and extracellular
53 states [7].

54 The micronemes are localized along the apical cortex in association with the subpellicular
55 microtubules emanating from the apical end [8, 9]. Upon activation of secretion, micronemes
56 move into the conoid, a tubulin basket at the very apical tip of the parasites, to fuse with the
57 plasma membrane. Following secretion, microneme protein complexes are embedded in the
58 plasma membrane with the extracellular domains serving as adhesion domains and the
59 cytoplasmic tail engaging with actin filaments that are transported in an apical to basal direction
60 by a myosin motor anchored in the membrane skeleton [10]. The working model is that
61 sustainable microneme secretion is dosed to support prolonged periods of gliding motility to
62 cross biological barriers in between host cells. Dosing is most likely achieved by gradually
63 trafficking micronemes aligned on the subpellicular microtubules toward the conoid to avoid
64 bulk micronemal content release. In addition, a set of radial micronemes organized and anchored
65 just below the conoid is believed to be a readily-releasable pool of micronemes [11-13].

66 Biogenesis of the micronemes and trafficking of microneme proteins progresses through
67 the secretory pathway comprising sequential passage through the endoplasmic reticulum (ER),
68 Golgi apparatus, trans-Golgi Network (TGN) and an endosome like compartment (ELC) [14-16].
69 Many secretory proteins undergo proteolytic processing to remove their pro-peptide mediated by
70 the plant like vacuole (VAC or PLV), an acidic compartment [17-20]. Protein sorting to both
71 microneme and rhoptry organelles requires sortilin (SORTLR) [21] whereas the
72 HOPS/CORVET complex and Rab7 are involved in PLV/VAC routing [22]. Moreover, adaptor

73 complex AP1 is involved in microneme and rhoptry protein trafficking, but has a more general
74 function across other vesicular trafficking events [23]. Although some rhoptry specific targeting
75 signals have been identified [24, 25], specific sorting signals for microneme proteins are still
76 elusive. Specific Rab GTPases have been associated with some aspects of microneme protein
77 trafficking, and actually differentiate two sub-populations of micronemes with a different protein
78 content: one of which is Rab5A/C-dependent, and one that is Rab5A/C-independent [9].
79 Consequently, specific microneme proteins end up in different, non-overlapping microneme sub-
80 populations. The exocytosis event at the very apical tip has been associated with Centrin2 [26]
81 and double C2 (TgDOC2) [27], both of which are Ca^{2+}-binding proteins. Furthermore, the
82 association of an acylated pleckstrin homology (PH) domain-containing protein (APH) on the
83 surface of the micronemes with PA deposited in the plasma membrane is essential for exocytosis
84 and aid in timing membrane fusion [28]. In addition, Rab11a is present at the very apical end of
85 the parasite and is required for efficient microneme exocytosis, though Rab11a's function is not
86 exclusively acting on the micronemes and is much more varied [29]. The proposed membrane
87 fusion model comprises v- and t-SNAREs on the microneme limiting membrane and the plasma
88 membrane, respectively, where TgDOC2, mediates the Ca^{2+} regulation, which together with
89 Rab11a and the APH-PA interaction pull the membranes together toward their fusion [6, 30].
90 However, the identity of such SNAREs is still elusive. Finally, sustained microneme secretion in
91 extracellular parasites is balanced with active endocytosis [31], whereas during cell division
92 micronemes of the mother are re-directed into the newly forming daughters [32].
93 In all the well-studied Ca^{2+} triggered exocytosis systems, proteins containing double C2,
94 (DOC2) domains execute the Ca^{2+}-mediated vesicle fusion [33]. C2 domains are approximately
95 150 amino acids in length and composed of eight beta strands that insert into a membrane or
96 associate with other proteins, some of which are conditional upon the presence of Ca^{2+} [33, 34].
97 Binding of Ca^{2+} and/or phospholipids is facilitated by specifically positioned residues in three
98 loops extending from the C2 domain. Aspartate residues, and to some extent glutamate, create a
99 negatively charged binding pocket that permits Ca^{2+} binding [35-37]. The binding of Ca^{2+} leads
100 to conformational changes facilitating insertion into a membrane or lipid binding via a calcium
101 bridge [38, 39]. Alternatively, asparagine in these positions, eliminates the negative charge, and
102 promotes phospholipid binding independent of Ca^{2+} [36, 37]. Typically, at least one membrane
103 associated and one soluble DOC2 protein are needed to facilitate Ca^{2+}-dependent fusion. We

104 have previously identified a soluble TgDOC2 protein essential for *Toxoplasma* microneme
105 secretion [27]. The ferlins make up a unique branch of the DOC2 domain protein family because
106 they are relatively large (200-240 kDa) and contain five to seven C2 domains rather than two,
107 which are typically organized in C2 pairs to form 2-3 DOC2 domains. The extended C2
108 repertoire in ferlins has broadened their functional spectrum beyond membrane fusion to vesicle
109 trafficking and membrane repair [40]. Mammalian ferlins come in two flavors differentiated by
110 their sub-cellular localization at either the plasma membrane or on intracellular compartments,
111 which relates to their function in either late endosomal transit versus trans-Golgi recycling [41].
112 Mammalian otoferlin, essential for neurotransmitter release from the inner hair cells (IHC) in the
113 auditory system, has been most widely studied. Otoferlin functions as both a scaffolding protein
114 in the secretory pathway as well as in the actual membrane fusion during exocytosis [42-45].
115 The Apicomplexa encode two conserved ferlin proteins, FER1 and FER2, but some
116 parasites, including *T. gondii*, encode a degenerate third ferlin [46]. FER1 in *Plasmodium*
117 *berghei,* named ferlin-like protein (PbFLP), was recently reported to be essential for male
118 gametocyte egress [47], whereas we showed that *Toxoplasma* FER2 is required for rhoptry
119 secretion [46]. Here we examined the function of FER1 in microneme protein trafficking,
120 microneme dynamics and secretion in the *Toxoplasma gondii* lytic cycle.
121
122
123 **Results**
124 **1. *Toxoplasma* FER1 localizes to the secretory pathway and a discrete apical region**
125 In the genome wide fitness screen for the *Toxoplasma* lytic cycle FER1 (TGGT1_309420) has a
126 severe fitness score of -4.77, strongly indicating that this protein is essential [48]. The critical
127 role of FER1 in the lytic cycle was underscored in our unsuccessful efforts to generate either an
128 endogenously tagged allele at either the N- or C-terminus to determine its sub-cellular
129 localization. Since FER1 is a tail-anchored transmembrane (TM) domain containing protein
130 ([49], Fig 1A), we reasoned that we could resolve its subcellular localization through fusion of
131 the terminal transmembrane (TM) domain including the extreme C-terminal cytoplasmic tail to a
132 YFP reporter. Transient transfection of parasites with an α-tubulin promoter driven fusion
133 construct encoding the C-terminal 31 aa (comprising the 10 aa before the extreme C-terminal and
134 the 21 aa long TM domain) resulted in YFP signal in an extremely apical, conoid-associated

135 region as well as in the perinuclear region (Fig 1B). This indicates that FER1 localizes to the
136 endoplasmic reticulum surrounding the nucleus as well as to the very apical tip of the parasite
137 from where microneme and rhoptry organelle exocytosis takes place. To corroborate these data,
138 we generated a polyclonal antiserum against the central C2DE domain (Fig 1A), which is the
139 most evolutionary diverse sequence of the protein compared to the other ferlins encoded by
140 *Toxoplasma*. By western blot, the affinity purified antiserum reacts with the full-length FER1
141 protein with a predicted molecular weight of 159 kDa. In addition, additional bands at
142 approximately 120 and 30 kDa were detected. These bands most likely represent fragments of
143 the full length FER1 protein, although cross reactivity with other proteins cannot be excluded.
144 However, the localization pattern of the α-FER1 serum by IFA resembles the pattern seen with
145 the YFP fusion to the TM domain of FER1, which suggests high specificity for FER1 in IFA
146 (Fig 1D,E). Again, we observe a very apical spot next to a perinuclear signal. To assess whether
147 the perinuclear localization extends beyond the ER we co-stained parasites with dynamin related
148 protein B (DrpB), a marker for the endosome like compartment (ELC) [50]. The ELC is a
149 structure in the secretory pathway past the Golgi apparatus and Trans Golgi Network (TGN) and
150 DrpB is critical for directing microneme and rhoptry proteins to their final destination [50].
151 Although direct co-staining is weak, the DrpB signal is seen right next to intense FER1 foci (Fig
152 1D), which suggests they could mark different compartments in the ELC. Together with the
153 continuous perinuclear stain these data indicate that FER1 distributes to the whole secretory
154 pathway including the Golgi apparatus. To elucidate the extreme apical regions to which FER1
155 localizes we co-stained parasites with antiserum against Vacuole Protein 1 (VP1). VP1 marks the
156 plant like vacuole (PLV) and acidocalcisomes in *Toxoplasma*, but an unspecified apical signal
157 near the conoid is also consistently observed [50-54]. We observe direct co-stain of FER1 and
158 VP1 in the apical tip of the parasite (Fig 1E). Finally, we co-stained extracellular parasites with
159 MIC2 antiserum to highlight the micronemes (Fig 1F). FER1and MIC2 signals were physically
160 distinct, with FER1 more apical than MIC2 in the micronemes. In extracellular parasites, the
161 FER1 signal was more exclusively localizing apical of the nucleus, suggestive of the Golgi, TGN
162 or ELC, contrasting with the peri-nuclear FER1 signal in intracellular parasites and suggesting a
163 dynamic pattern for FER1. Taken together, FER1 localization at the apical VP1 compartment of
164 unknown identity is seen in both intra- and extra-cellular parasites, whereas FER1 marks the
165 entire ER to ELC pathway in intracellular parasites but is absent from the ER in extracellular

166 parasites. FER1's localization pattern in *T. gondii* is consistent with mammalian ferlins
167 functioning in late endosomal transit versus TGN recycling [41], since trafficking to the rhoptries
168 and micronemes in the Apicomplexa is facilitated by a modified endosomal system [15, 16].
169
170 **2. Generation and validation of conditionally lethal FER1 mutant lines**
171 To dissect the function of FER1 we followed a dominant negative (DN) approach. We
172 anticipated that conditional overexpression of an allele without the C-terminal TM domain would
173 mislocalize FER1, divert its interacting proteins, and disrupt its function. We generated an α-
174 tubulin promoter driven N-terminal fusion of the destabilization domain (DD) linked to a Myc
175 epitope that can be conditionally stabilized with Shield-1 [55]. We designed both an allele
176 without the 21 C-terminal amino acids encoding the TM domain (DD-Myc-FER1ΔTM) as well
177 as a control construct encoding the full-length FER1 protein (DD-Myc-FER1^{FL}) (Fig 2A). We
178 were able to generate stable parasite lines with both constructs in absence of Shield-1.
179 Expression of the full-length proteins was assessed by western blot, showing higher FER1 levels
180 already in the absence of Shield-1 as the lower MW bands seen in wild type parasites were not
181 observed at the exposure time needed to detect the overexpressed protein (Fig 1C, 2B). Next, we
182 showed by plaque assay that overexpression of both the ΔTM and FL alleles caused a severe
183 fitness defect (Fig 2C). These observations underscore a critical role of FER1 in the lytic cycle as
184 seen in the genome wide CRISPR screen [48].
185
186 **3. FER1ΔTM overexpression causes a microneme secretion defect**
187 To globally determine the cause of the lethal defect upon FER1ΔTM overexpression we
188 evaluated the following key events of the lytic cycle: host cell invasion (Fig 3A), replication (Fig
189 3B,C), and host cell egress (Fig 3D-F). Host cell invasion was strongly reduced, consistent with
190 an anticipated FER1 role in invasion through microneme content exocytosis. We observed a mild
191 reduction in the parasite multiplication rate, with a slight but significant (p=0.031) accumulation
192 of parasites in the 4-cells/vacuole stage compared to the controls (Fig 3B). We did not detect a
193 specific delay in a particular cell cycle stage (Fig 3C), suggesting that the overall rate through
194 cell division is somewhat reduced. As summarized in Fig 3D, we triggered egress by several
195 different secretagogues, engaging the signaling pathway toward egress at different points: most
196 upstream is zaprinast to activate protein kinase G (PKG), followed by ethanol activating

197 phosphoinositide phospholipase C (PI-PLC) right before the bifurcation in a Ca^{2+}-dependent
198 (triggered with Ca^{2+}-ionophore A23187) and phosphatidic acid (PA) dependent pathway
199 (triggered with phosphatidic acid phosphatase (PAP) inhibitor propranolol) [28]. We monitored
200 egress by assessing the integrity of the parasitophorous vacuole membrane (PVM) using GRA3
201 as PVM marker and the parasite's cytoskeleton marker IMC3 for parasite dispersal in the
202 environment (Fig 3F). None of these secretagogues efficiently induced egress (Fig 3E). To
203 determine whether the defect was specific to egress as observed in CDPK3 signaling mutants
204 [56-58], we permeabilized the plasma membrane with saponin. This bypasses the signaling step
205 specific for egress and triggers the activation of motility by the extracellular environment.
206 Although this did not trigger egress in the FER1ΔTM overexpressing mutant, we noticed loss of
207 PVM integrity upon overexpression. Even though saponin might contribute to this effect, this
208 observation is suggestive of modest microneme release. We performed trail assays as a
209 functional and independent assay to assess microneme secretion, and determined that it is
210 insufficient to support gliding (Fig 3G). Finally, we determined differential microneme secretion
211 from the Rab5A/C-dependent (MIC3, 5, 8) and -independent (MIC2, MIC10, M2AP, PLP1, etc.)
212 microneme sub-populations [9]. The former sub-population was tested by release of processed
213 MIC2 in the medium under various exocytosis triggering conditions, whereas the latter was
214 visualized by MIC3, 5 and 8 protein exposure on the parasite's surface. Overall, we see a sharp
215 reduction in secretion from both microneme populations in the FER1ΔTM overexpressing
216 mutant to nearly undetectable levels. However, we reproducibly detected propranolol induced
217 secretion at a 10-fold lower level than in the non-induced control (a drop from 161% to 15%
218 relative to the total 10% total microneme control; Fig 3H). In addition, we observed a very small
219 amount of MIC3 on the surface of induced parasites, indicating that this population still has
220 minor secretion capacity as well (Fig 3I). Since propranolol triggers the PA pathway, which is
221 independent of the Ca^{2+}-dependent leg (Fig 3D), this section of the pathway appears to be still
222 functioning, albeit at a very low level. Taken together, this suggests that FER1 acts primarily in
223 the Ca^{2+}-dependent events in the micronemal secretory pathway.
224
225 **4. FER1ΔTM overexpression causes a microneme trafficking defect**
226 By design, we anticipated that FER1ΔTM would mislocalize. Using the Myc-tag in the
227 overexpression DD-Myc-FER1ΔTM construct in IFA revealed a striking accumulate in a defined

228 mid-apical region, within a background of lower intensity Myc dispersed throughout the
229 cytoplasm also seen in absence of Shield-1 (Fig 4A). We reasoned that the background Myc
230 signal is likely due to proteasome degraded fragments present throughout the cytoplasm. We
231 addressed this concern by overexpressing a YFP version since YFP fragments generated by the
232 proteasome would not autofluorescence. Indeed, we observe no YFP signal without Shield-1
233 whereas under Shield-1 we see a similar signal in the mid-apical region as seen with the Myc-
234 tagged version. Therefore, we used the YFP version for all subsequent imaging experiments. Co-
235 staining with several microneme proteins in the Rab5A/C-dependent (MIC5 stained) and -
236 independent (MIC2 stained) class showed perfect overlap with the accumulated YFP signal
237 suggesting all microneme proteins are misdirected (Fig 4B,C, S2A,B). The FER1 antiserum
238 signal also co-localizes with the YFP signal. This could suggest that endogenous FER1 may also
239 be diverted from its apical tip and peri-nuclear enrichments to the accumulation of dominant
240 negative FER1ΔTM (Fig 4D), although we cannot rule out the possibility that the massively
241 overexpressed FER1ΔTM as seen by western blot (Fig 2B) overwhelms the endogenous signal.
242 Collectively, these data indicate that both the Rab5A/C dependent and independent microneme
243 sub-populations are controlled by FER1. Since all known microneme protein trafficking mutants
244 in the endosomal sections have concurrent defects in rhoptry protein trafficking [18], we
245 interrogated the rhoptries by IFA. We observed that the ROP proteins remained localized to
246 rhoptries, and that the rhoptries displayed their normal morphology and distribution (Fig 4E).
247 This striking distinction makes the DN-FER1 phenotype a first of its kind for the unique
248 disruption of microneme trafficking while leaving the rhoptries intact.
249 The central apical localization is reminiscent of the position of various compartments of
250 the *Toxoplasma* secretory pathway. To differentiate whether the accumulation is due to an arrest
251 in trafficking, mis-trafficking, or is of another nature we used a series of secretory pathway
252 specific compartment markers in co-localization experiments (Fig 4F, G). First, we checked
253 whether the FER1 co-localization with PLV/VAC compartment using VP1 as marker. We
254 observe no overlap at all between the VP1 and YFP signals (Fig 4F). We observed similar lack
255 of co-localization with PLV/VAC compartment using NHE3 as an independent marker of this
256 compartment [54] and show that it still displays its normal morphology (Fig S2C). However, we
257 noted that the VP1 signal at the apical end is still very prominent (Fig 4F). Surprisingly, we
258 never observed co-localization of the mid-apical DD-YFP-FER1ΔTM signal with the Golgi

259 apparatus, TGN, or the ELC, which all displayed their normal morphology. Instead, DD-YFP-
260 FER1ΔTM accumulated in a uncharacterized compartment, beyond any of the known trafficking
261 steps toward the micronemes, and after the split from rhoptry protein trafficking [18].
262 To reveal the sites of DD-YFP-FER1ΔTM and microneme protein accumulation, we
263 performed transmission electron microscopy (Fig 4H-M). EM studies illustrate that in DD-YFP-
264 FER1ΔTM-expressing parasites, micronemes with normal ultrastructure were not decorating the
265 cytoplasmic side of the cortical cytoskeleton at the apical end but instead were aggregated in the
266 cytoplasm at the apical region of the parasite (Fig 4H). In addition, we observed electron-lucent
267 compartments that in several cases contained electron-dense material (Fig 4I, J). We further
268 investigated the content of these enlarged compartments with possible microneme connection by
269 immunolabeling the parasites with α-MIC2 antibody. Gold particles positioned MIC2 in the
270 aggregated microneme structures (Fig 4K) as well as on the outside edges of the electron-lucent
271 compartments and within the electron-dense spheres within the electron-lucent compartments
272 (Fig 4L,M). The MIC2 association and the appearance of electron dense structures is consistent
273 with the function shared between the ELC and PLV/VAC compartments previously reported [17,
274 59]. Although these compartments appear enlarged, they are likely part of the physiological
275 trafficking pathways of microneme proteins. In summary, overexpression of dominant negative
276 FER1ΔTM leads to mislocalization of fully mature micronemes without disrupting the
277 trafficking pathway or the biogenesis of the rhoptries. These data indicate that FER1 functions in
278 the trafficking and/or biogenesis of micronemes beyond the ELC, which is the least understood
279 step in microneme biogenesis and secretion [14].
280
281 **5. DD-YFP-FER1ΔTM overexpression retracts micronemes from the periphery**
282 We tested whether the aggregated micronemes in the mid apical region observed by EM did
283 complete their biogenesis by staining with a marker present on mature micronemes: acylated
284 pleckstrin-homology (PH) domain-containing protein (APH). APH on the microneme's surface
285 senses PA during microneme secretion and is necessary for microneme exocytosis [28]. Indeed,
286 APH co-localized with the site of FER1 accumulation in both intra- and extra-cellular parasites
287 which indicates that the mis-localized micronemes, for signaling purposes, are primed for
288 secretion as in non-induced parasites (Fig 5A). In addition, in extracellular parasites we
289 frequently observed a specific APH signal at the very apical end of the parasite (arrowhead in

290 Fig 5A). These likely represent a small microneme population that can still be secreted,
291 consistent with the 10% residual microneme secretion in induced parasites (Fig 3H,I). In
292 addition, as guided by the EM data, we asked whether the microneme proteins are fully matured,
293 i.e. completed proteolytic processing by removal of the pro-peptide in the ELC/VAC
294 compartment [17, 20]. We used specific antisera against the pro-peptide of M2AP together with
295 antiserum reacting with the mature M2AP protein [60]. By western blot we observe no
296 difference in relative abundance of the pro-M2AP protein versus the total amount of M2AP
297 protein across all conditions and mutants tested (Fig 5B). Furthermore, by IFA we observe
298 normal MIC5 pro-peptide containing proteins in the ELC compartment [60], and no co-
299 localization with the FER1 accumulation (Fig 5C). These observations further support that the
300 mislocalized micronemes contain mature proteins that completed processing through the
301 secretory pathway.
302 Since pro-MIC5 manifests predominantly in budding parasites, the co-staining with FER1
303 revealed another intriguing phenomenon: there appeared to be no DD-YFP-FER1ΔTM
304 accumulation in newly forming parasites. We validated this model by a triple staining with YFP,
305 α-pro-MIC5 and daughter bud marker α-IMC3 (Fig 5D). Moreover, representative images
306 through the division cycle demonstrate that the YFP migrates basally toward the residual body in
307 parasites undergoing division (Fig 5E). Moreover, we never observed any new micronemes in
308 the apical peripherally of daughter buds either (Fig 5F). Collectively, these data indicate that
309 microneme pro-protein processing by the ELC/VAC compartment progresses normally in newly
310 forming daughters, yet new micronemes do not assemble in the daughters, suggesting microneme
311 proteins end up in the YFP-FER1ΔTM pile up formed in the mother. This raised the next
312 intriguing question: is the YFP aggregation independent of cell division? This model implies that
313 normally localized micronemes can be retracted from the periphery and directed toward the YFP
314 microneme aggregate. To this end we performed time courses to determine induction and
315 reversion kinetics of the Shield-1 induced phenotype in both intracellular and extracellular
316 parasites. Microneme mis-localization kinetics were over 95% complete within three hours (Fig
317 5G top panel). This time frame is much smaller than the 6.5 hr cell division cycle, indicating that
318 the process is not cell cycle dependent as in an unsynchronized population typically 30% of the
319 parasites is undergoing daughter budding [61]. The exact same kinetics were also observed in
320 extracellular parasites which are arrested in a non-division G1/0 state (Fig 5G bottom panel).

321 What was even more striking is that the phenotype is completely reversible with kinetics very
322 comparator to induction (Fig 5G). Finally, to directly visualize the cell division independent re-
323 localization of the micronemes we performed time lapse microscopy following Shield-1
324 induction. In DD-YFP-FER1ΔTM co-expressing a MIC3-mCherryRFP marker we observed that
325 microneme retraction and accumulation with YFP-FER1ΔTM started after 1.5 hr of Shield-1
326 induction (Supplementary Movie S1 and Fig 5H). Moreover, time lapse imaging confirmed that
327 microneme retraction was independent of daughter budding as tracked with a marker enriched in
328 daughter cytoskeletons, IMC3-mCherryRFP (Supplementary Movie S2 and Fig S3). Taken
329 together, overexpression of a dominant negative FER1 allele induces retraction of already
330 correctly localized micronemes from the periphery toward a centrally localized organelle
331 accumulation regardless of cell division cycle stage. The reversible nature of the FER1 mediated
332 process indicates that whole organelle microneme trafficking in principle is bidirectional from
333 where they are docked on the subpellicular micronemes to the site of apical aggregation beyond
334 the known secretory pathway compartments. Therefore, our data reveal that microneme
335 trafficking can in principle be bidirectional and might not be exclusively targeted toward the
336 apical end in support of exocytosis.
337
338 **6. FER1^{FL} overexpression results in premature, untriggered microneme secretion**
339 The precarious nature of FER1 function was evident from the lethal effect of DD-Myc-FER1^{FL}
340 overexpression (Fig 2C). We dissected this phenotype first by assessing the localization of
341 FER1, which is largely unchanged upon Shield-1 induction and presents on membrane structures
342 throughout the parasite. (Fig 6A). Next, we asked whether these parasites display changes in
343 their microneme secretion ability using the set of secretagogues applied to the ΔTM mutant. We
344 observe strong exocytosis under all conditions, compared to the negative DMSO control (Fig
345 6B). Although we see slight variations in the sensitivity to different secretagogues compared to
346 the non-induced and wild type parasites (Fig S1), they were not significant and unlikely
347 responsible for the lethal phenotype.
348 Next, we focused on microneme localization and morphology by IFA. We first assessed
349 the Rab5A/C-dependent sub-population using MIC5 and MIC8 as representatives. In non-
350 induced parasites these display the typical microneme pattern. Upon full-length FER1
351 overexpression, a dissociation of Rab5A/C-dependent microneme sub-population from the

352 subpellicular microtubule was observed, but the most apical microneme localization remained
353 (Fig 6C). Staining for the Rab5A/C-independent population with MIC2 again revealed a change
354 in localization pattern, but this was dramatically different from the MIC8 population. By super-
355 resolution SIM, in induced intracellular parasites the microneme signal was strongly
356 concentrated at the apical end, unlike the tapering signal observed in wild type and non-induced
357 controls (Fig 6D top panels). These extremely apical micronemes, also maintained for the
358 Rab5A/C-dependent population, are reminiscent of the radial micronemes organized just below
359 the conoid [12]. The radial micronemes are anchored firmly in the apical region and believed to
360 be primed for secretion [11]. In extracellular parasites however, we did not notice dramatic
361 changes between the induced mutant and the controls: under all conditions MIC2 was more
362 shifted apically compared to the intracellular wild type distribution, yet not so radically apical as
363 in the intracellular induced mutant parasites (Fig 6D lower panels). To obtain an even higher
364 resolution visual on the micronemes in this mutant we resorted to both IEM and TEM. Here we
365 observe an accumulation of micronemes at the apical end, confirming the apical MIC signals
366 seen by light microscopy (Fig 6E, F). Several micronemes were squeezed inside the conoid,
367 whereas the densely packed micronemes in the apical region just below the conoid often
368 displayed an elongated morphology. Further below, we do see scattered micronemes, which
369 likely were the MIC8 micronemes as observed by IFA. Thus, it appears overexpression of N-
370 terminally tagged, full-length FER1 has a differential effect depending on the population of
371 micronemes set apart by Rab5A/C dependence: the MIC2 population is driven to the apical end,
372 whereas the MIC8 population becomes more scattered. Taken together, this is suggestive of a
373 role for FER1 in directing micronemes along the subpellicular microtubules toward the conoid.
374 To gain further insights in this phenotype we tested specific functional capacities of these
375 apically concentrated micronemes. We first showed that swift parasite egress could be triggered
376 by Shield-1 addition alone (Fig 6I). Egress implies microneme secretion, which we subsequently
377 tested under intracellular conditions in Endo buffer [62]. Release of MIC2, albeit weakly, was
378 observed upon Shield-1 induced egress (Fig 6J). However, we never observed robust levels of
379 MIC2 release, suggesting that only a small pool of micronemes can be released immediately
380 upon Shield-1 treatment. However, already a small amount of micronemal protein release could
381 lead to parasitophorous vacuole membrane permeabilization due to the action of perforin like
382 protein 1 (PLP1) secreted from the micronemes [4]. To further test the FER1 mediated

383 microneme release capacity independent of other signaling triggers we tested whether egress
384 could be triggered in small vacuoles, which have not yet established an acidified PVM [5] or
385 accumulated secreted diacylglycerol kinase 2 (DGK2) inside the PV [63], both of which are
386 required for natural egress [6]. To this end we modified the standard red-green invasion assay
387 into an invasion+egress assay exploiting the same differential staining of intracellular vs
388 extracellular parasites [64]. Following 1 hr standard invasion, non-invaded parasites were
389 washed away and Shield-1 added for two hrs (Fig 6K top). Nearly 50% of vacuoles with single
390 parasites have egressed (Fig 6K bottom), which largely mimics the 60% egress rate seen after 2
391 hrs of induction from large vacuoles. Collectively, these data strongly support that Shield-1
392 induced microneme secretion is only due to FER1 and not due to activation of the generic
393 signaling pathways leading to egress.
394
395 **7. Putative Ca^{2+}-binding residues are critical for FER1 function**
396 To probe the mechanism of FER1 beyond the TM domain we analyzed the individual C2
397 domains for their functional potential. C2 domains fold into β-sheets connected by three loops
398 that can bind to proteins or insert in membranes, which can be modulated upon binding Ca^{2+} [33,
399 34, 38, 39]. Five key residues in the loops, of which the three central ones carry most weight
400 [37], can predict an association with phospholipids in membranes or Ca^{2+}. Across the C2
401 domains in FER1, we only detected Ca^{2+}-binding potential in the C2D domain which carries
402 three Asp residues and a supportive Glu residue in the conserved loop positions which
403 potentially can stabilize two Ca^{2+} ions (Fig 7A,B). We tested the contribution of the C2D domain
404 to FER1 function by mutating two of the conserved Asp residues in loop 1 to Ala, which is
405 predicted to disrupt binding both Ca^{2+} ions (Fig 7B). We conditionally overexpressed the mutant
406 FER1 allele carrying the D541A and D545A mutations in the same N-terminal DD fusion
407 context of a ΔTM or full-length allele. We were unable to express either alleles stably within
408 parasites, even in absence of Shield-1, which indicates that these C2D residues are very critical
409 to FER1 function. Instead we performed transient transfections to analyze the consequences of
410 these mutant alleles on the parasite (Fig 7C, D). Expression levels of the transgenes under
411 Shield-1 were high as vacuoles positive for both Myc and α-FER1 staining clearly stand out in
412 both channels. However, in Myc negative vacuoles the endogenous FER1 was not discernable
413 under the settings used to optimally display the FER1 signal in overexpressing parasites,

414 indicating that expression of the mutant allele is well above endogenous FER1 levels. Most
415 notable however, the aggregated FER1 signal was not seen upon overexpression of the wild type
416 FER1ΔTM allele, indicating that the C2D domain is critical in mediating this phenotype.
417 Overall, the overexpressed full-length DD-Myc-FER1^{FL}-$^{(D541A,5D45A)}$ pattern is similar to the wild
418 type allele and localizes to various focal membrane structures.
419 Subsequently, we used representative antisera to assess both the Rab5A/C-dependent
420 (MIC8) and -independent (MIC2) microneme sub-populations by IFA. For the DD-Myc-
421 FER1ΔTM$^{(D541A,D545A)}$ a difference between the two microneme sub-populations was noticeable:
422 the morphology and intensity of the Rab5A/C independent micronemes were indiscernible in
423 non-transfected parasites (MIC2; yellow circle in Fig 7C). However, the Rab5A/C-dependent
424 micronemes became apically defined and strongly concentrated (MIC8; white circle in Fig 7C).
425 This presentation strongly mimics the pattern seen for overexpression of the full-length wild type
426 allele (Fig 6C). Thus, it appears that the Rab5A/C-dependent micronemes do not need a
427 functional FER1's C2D domain to traffic to the apical conoid region upon FER1 overexpression.
428 In DD-Myc-FER1$^{FL-(D541A,D545A)}$ overexpressing parasites we do not observe a difference
429 between the microneme sub-populations by IFA. Interestingly, both microneme populations lose
430 their staining intensity compared to wild type parasites (Fig 7D, white circles). Collectively, this
431 indicates that the conferred function of domains in FER1 can change upon the context of the
432 whole proteins, e.g. by certain domains being present or absent (e.g. TM domain), accessible
433 (e.g. N-terminal fusion) or functional (Ca^{2+}-binding).
434
435
436 **Discussion**
437 Our findings and insights are summarized in Fig 8 and support several roles for FER1 in the lytic
438 cycle, 1. Microneme protein trafficking between the ELC to the subpellicular microtubules; 2.
439 Directing the micronemes assembled on the subpellicular microtubules forward to the apical end
440 in extracellular parasites; 3. Transport into the conoid and membrane fusion between the
441 microneme and plasma membranes to facilitate exocytosis; 4. From the bi-directional and
442 completely reversible transport of the micronemes from the subpellicular microtubules to a
443 luminal position we infer that the functional relevance of this feature resides in the recently
444 reported microneme recycling from the mother parasite in daughters under assembly [32]. The

445 dual localization pattern of endogenous FER1 (Fig 1) together with reports on the connection
446 between localization pattern and human ferlins [41] are consistent with these roles: FER1 in the
447 TGN/ELC is responsible for trafficking to (and from) the anchoring site on the subpellicular
448 microtubules, whereas FER1 in the apical end co-localizing with VP1 facilitates fusion with the
449 plasma membrane. Consistent with the tail-anchored transmembrane model [49, 65], just the TM
450 domain fused to a reporter mimics endogenous FER1 localization. Together with the mis-
451 localizing microneme phenotype upon overexpression of the ΔTM allele, we assert that the TM
452 domain is associated with microneme organelle trafficking. Further support for this interpretation
453 is provided by the vesicular localization in the gametocyte cytoplasm reported for the FER1
454 ortholog PbFLP in *P. berghei* [47].

455 The kinetics of microneme mislocalization upon overexpression of the DN ΔTM allele
456 provided additional tantalizing insights. Our extensive marker set together with the ultrastructure
457 established beyond a doubt that the aggregated micronemes are fully mature and contain fully
458 processed proteins. Most importantly, we show that completely mature micronemes at any point
459 in the cell cycle in intracellular parasites as well as in extracellular parasites are released from the
460 subpellicular microtubules and traffic back to a cytoplasmic location apical of known secretory
461 pathway compartments where they aggregate. Although similar appearing microneme pile ups
462 were recently reported upon the disruption of the vacuolar-proton ATPase (v-ATPases) in
463 *Toxoplasma*, they contained microneme proteins from which the pro-peptide had not been
464 cleaved [20] and thus do not represent mature micronemes like we observed. However, these
465 data support the notion that microneme morphology appears to be complete before they traffic
466 toward the subpellicular microtubules. Indeed, trafficking of micronemes from mother to
467 daughters was recently reported as well [32], which further supports the feasibility and a
468 biological function for the retrograde microneme organelle transport we observe. Moreover, the
469 effect we see is specific for the micronemes, unlike most other mutants in the endosomal legs of
470 microneme trafficking, which invariable also affect rhoptry protein trafficking (e.g. [21, 23]).
471 Overall, FER1 provides the first mechanistic insight in the microneme specific trafficking after
472 the trafficking pathway diverges from the upstream route shared with the rhoptries.

473 Overexpression of the full-length FER1 supports a direct role in membrane fusion in the
474 actual exocytosis. The first piece of evidence is that Shield-1 induction leads to fast egress of
475 parasites in vacuoles (Fig 6I,K). This invariably requires microneme secretion, and we directly

476 detect microneme secretion, albeit modest, under intracellular conditions (Fig 6J). This modest
477 release is sufficient to drive egress, but secretion is not sustained, which requires activation of
478 the complete signaling pathway of secreted micronemes (Fig 6B). Thus excess FER1
479 compensates for other requirements for membrane fusion, such as APH engagement with PA in
480 the plasma membrane [30]. In parallel to other secretory systems [66, 67], we believe that only
481 the primed or so-called readily-releasable microneme pool is released in this mutant, but that
482 additional secretion requires renewed priming (e.g. Ca^{2+}-dependent events such as potential
483 phosphorylation of FER1 [68]), which only occurs when the complete signaling cascade is
484 engaged. The so-called radial micronemes which are accumulated right below the conoid make a
485 good candidate for this readily releasable microneme pool [12, 13]. The radial micronemes are
486 tightly anchored as they were the only set of micronemes remaining upon VPS9 knock-down
487 [11]. However, technically we cannot exclude that only one or two micronemes are present as
488 pre-docked micronemes at the plasma membrane and are engaged to complete fusion with the
489 plasma membrane upon FER1 overexpression.
490 An additional phenomenon observed upon FER1 overexpression is that the MIC2
491 microneme population squeezes into the apical end of the parasite, indicating transport was
492 triggered as well. A similar microneme apical migration phenotype was observed upon knock out
493 of the clathrin adaptor protein AP1, although that was not unique to the micronemes and acted
494 much more widely across many aspects of vesicular trafficking, including cell division [23]. But
495 it indicates that FER1 and AP1 both act in the same pathway that facilitates movement of some
496 micronemes to the apical end of the parasite. Since the AP1 mutant did not lead to microneme
497 secretion, we conclude that the short secretion burst, and apical movement are independent
498 events facilitated by FER1 overexpression. Phenomenologically, we interpret the apical
499 movement as part of the process of secretory vesicle replenishment. By comparison, in mammals
500 a role for otoferlin in replenishment of synaptic vesicles is supported, which mimics this
501 particular function of FER1 in *Toxoplasma* [13, 45, 69].
502 Our data on FER1 indicate that the TM domains is needed to anchor FER1 in early
503 segments of the secretory pathway (ER, Golgi, TGN, ELC). C2 domain analysis of FER1 only
504 pointed at C2D with potential for Ca^{2+} binding and no strong indicators of potential phospholipid
505 binding were identified. Among mammalian ferlins, the C2D domain of otoferlin has been
506 demonstrated directly to bind Ca^{2+} [42] and interacts with MyosinVI [70] to enable vesicle

507 transport [43]. In general, low Ca^{2+} promotes intramolecular protein-protein interactions among
508 otoferlin C2C, C2D, C2E, and C2F domains, whereas high Ca^{2+} triggers a conformational switch
509 and leads to interaction with phospholipids [43] and SNARE proteins *in vitro* [71, 72].
510 Translated onto *Toxoplasma* FER1, these observations and our analysis suggest that the C2
511 domains function in intra-molecular protein-protein interactions to expose or hide functional
512 domains conditional upon signaling conditions. Indeed, depending on the FER1 mutant used, we
513 observe distinct effects on the Rab5A/C-dependent and -independent microneme populations.
514 For example, upon full-length overexpression we observe the Rab5A/C-independent micronemes
515 (MIC2) moving forward without a notable change in the Rab5A/C-dependent micronemes
516 (MIC5/8), whereas without the TM, the C2D Ca^{2+}-binding sites are needed to drive the MIC5/8
517 micronemes apically, suggesting the TM acts differentially on these microneme subsets. The
518 C2D Ca^{2+}-binding sites promote apical microneme migration along the subpellicular
519 microtubules. In addition, an intact C2D domain is needed to either maintain or form the MIC2
520 micronemes (we cannot differentiate between these two scenarios). The complex patterns of
521 dynamic and differential changes suggest a model wherein different FER1 domains modulate
522 each other's function dependent on the context: e.g. the C2D domain binds to other C2 domains
523 within the FER1 proteins and stabilizes a certain protein fold consistent with one of FER1's
524 different functions. There are ample signaling events associated with the micronemes that may
525 act to expose, shield, and/or activate other C2 domains in FER1 [6], such as phosphorylation by
526 CDPK1 [73], PKA [7] or PKG [74, 75], binding of DOC2 upon high Ca^{2+} [27] and/or lipids
527 becoming available in the signaling pathway due to PAP activity [28] or the guanylate-cyclase-
528 flippase localized at the apical plasma membrane [63], toward membrane fusion competence.
529 Incapacitating Ca^{2+}-binding in the C2D domain changes FER1 activity in intracellular
530 parasites which have a low cytoplasmic Ca^{2+} concentration. This suggests that this domain has a
531 high affinity for Ca^{2+}. Given the absence of critical amino acids able to stabilize Ca^{2+} in the other
532 C2 domains, it is unlikely that FER1 bind Ca^{2+} with a low affinity when the signal transduction
533 pathway is engaged. However, in Synaptotagmin-1, a mammalian DOC2 protein, conserved Asp
534 residues in the C2A domain interacts with those in C2B, thereby creating a single Ca^{2+} pocket in
535 the DOC2 domain [76], which might apply to FER1. Alternatively, high Ca^{2+} concentration
536 might be transduced by the soluble TgDOC2 protein, which has also been shown to be critical to
537 microneme secretion [27]. In this scenario, paralleled in neurotransmitter release [77], a raise in

538 cytoplasmic Ca^{2+} would drive TgDOC2 to interact with the membrane fusion complex at the
539 primed, radial micronemes as the critical Ca^{2+}-mediated step in membrane fusion and exocytosis.
540 A caveat from dominant negative allele overexpression studies is that they are generated
541 in presence of an intact endogenous allele. The overexpression of the N-terminally tagged wild-
542 type allele resulted somewhat surprisingly in a cytoplasmic localization. Possibly, the N-terminal
543 fusion blocks functionality requiring an accessible FER1 N-terminus, or alternatively, the high
544 level of overexpression saturates the secretory pathway driving the protein into the cytoplasm.
545 Although the second scenario is supported by the higher level of overexpressed protein
546 compared to the ΔTM allele, where we do not observe a cytoplasmic signal, access to the N-
547 terminus is likely essential as well. We were unable to obtain stable parasite lines where
548 endogenous FER1 was tagged on either the N- or C-terminus. Neither were we able to generate
549 parasite lines with conditional alleles using any of the systems available in *Toxoplasma*
550 (tetracycline regulatable promoter replacement or replacing the 3'-UTR with the conditional U1
551 snRNP motif). Even though a C-terminal tagged PbFLP was stable in *P. berghei* [47], we
552 conclude that in *Toxoplasma* tachyzoites the amenability of FER1 to manipulation has an
553 extremely narrow bandwidth. We successfully bypassed this obstacle by generating antisera
554 against FER1 for localization studies, and the overexpression of dominant negative alleles to
555 determine FER1 function.
556 Another intriguing question generated by our study is the nature of the co-localization of
557 FER1 and VP1 at the apical end. All insights on ferlins in general together with our data suggest
558 that FER1 is microneme associated, which would suggest this signal most likely corresponds
559 with the radial micronemes. Ergo, why is there VP1 in the radial micronemes? VP1 is associated
560 with the acidocalcisomes [78], which it acidifies, as well as with the PLV/VAC [51], where its
561 function is less clear as a distinct v-ATPase acidifies that compartment [20]. This suggests that
562 acidification of the radial micronemes might precede their secretion. Indeed, acidification of the
563 readily releasable vesicle pool is a priming mechanism described in a variety of secretory
564 systems, including neurotransmitter [79] and insulin release [80-82]. In these systems
565 acidification is facilitation by a v-ATPase. Whether VP1 is a functional replacement of this
566 function in *T. gondii* is as yet an untested aspect of this model. Either way, the exact role of the
567 v-ATPase is debated as it has also been shown to act more as a pH sensor [83, 84]. Our
568 observation that VP1 remains apically when all micronemes aggregate upon ΔTM

569 overexpression could suggest a dynamic composition of this compartment, although we cannot
570 exclude that endogenous FER1 still co-localizes with VP1 under these conditions. This latter
571 scenario fits with our observation that a small pool of micronemes remains sensitive to
572 propranolol induced secretion, which must reside apically to be secreted.
573 Additional players with related apical localization patterns comprise Rab11a [29].
574 Depletion of Rab11a reduces motility [85], whereas overexpression of a dominant negative allele
575 reduces MIC2 secretion [29]. But Rab11a's main function is in dense granule secretion with an
576 additional role in cell division [86], which therefore makes its role pleomorphic and complicates
577 to drawing direct connections between Rab11a and FER1 events. Such pluriform role is akin to
578 the defect in microneme apical movement seen upon the knock-out of AP1 [23]. Further
579 strengthening a putative ferlin – Rab11 connection is based on a similar observations for human
580 ferlin Fer1L6, which cycles between the PM and trans-Golgi/recycling endosomes via Rab11
581 recycling endosomes [41]. Therefore, a connection between *T. gondii's* Rab11a and FER1 at the
582 actual microneme secretion step is quite likely.
583 Centrin2 is another player at the apical tip of the parasite with multiple additional
584 localizations in the parasite (centrosome, apical annuli, basal complex) that was recently
585 connected to microneme secretion [26, 87]. Furthermore, a centromeric protein, Chromo1, is also
586 present at the same apical localization, but a putative role with microneme secretion has not been
587 explored [23]. Finally, a conserved phosphoinositide-binding protein, PfPH2, was shown in *P.*
588 *falciparum* to act on a limited set of microneme proteins, although different populations of
589 micronemes have not been demonstrated in *Plasmodium* [88]. Moreover, PfH2 localizes close to
590 the apical tip or merozoites, not unlike where FER1 and VP1 co-localize. The paucity in our
591 understanding of microneme secretion is the putative role of SNARE proteins at the site of
592 exocytosis [18]. Although it has been extensively reported that ferlins interface with SNAREs in
593 membrane fusion [44, 71, 72], auditory hair cells might release vesicles mediated by otoferlin
594 without SNAREs [89]. Furthermore, it has been postulated that fast, Ca^{2+}-dependent exocytosis
595 is inconsistent with the role of SNAREs [90] and some exocytosis in absence of SNAREs is
596 possible [91]. Some neurotransmitter is still released when all relevant SNAREs are depleted
597 [91], and indeed, alternative models for SNARE independent neurotransmitter release have been
598 postulated [90]. Indeed, the multiple C2 domains in ferlins have been proposed to be able to
599 support membrane binding integrating the Ca^{2+}-sensing and membrane fusion events [40, 92]

600 and as such FER1 might act in absence of SNAREs in *Toxoplasma*. Taken together, a
601 conglomerate of molecular players at the apical end has been identified with roles in microneme
602 exocytosis. Direct links between the observations will be an exciting avenue for future work.
603 By integrating the new insights generated in this study we propose a model of microneme
604 exocytosis wherein the radial micronemes constitute a readily releasable vesicle pool primed by
605 acidification as shown in Fig 8. Several aspects of this model remain to be tested, and whether it
606 holds up or not, the eclectic collection of molecular players assembling at the site of microneme
607 secretion predict many as yet unanticipated events to be discovered.
608
609
610 **Material and Methods**
611
612 **Parasites and host cells**
613 Transgenic derivatives of the RH strain were maintained in human foreskin fibroblasts (HFF) or
614 hTERT immortalized HFF cells as previously described [93]. Parasite transfections and
615 selections use 1 µM pyrimethamine, 20 µM chloramphenicol, 5 µg/ml FUDR, or a combination
616 of 25 mg/ml mycophenolic acid and 50 mg/ml xanthine (MPA/X). All parasite lines were cloned
617 by limiting dilution.
618
619 **Generation of constructs and parasite lines**
620 All primer sequences are provided in Supplementary Table S1; all plasmids used are provided in
621 Supplementary Table S2. Expression plasmids fusing ddFKBP destabilization domain (DD) with
622 FER1 were generated from tub-DD-Myc-YFP/sagCAT plasmid [55] by replacing YFP with the
623 PCR amplified FER1 CDS (primer pair 1573/1574) by AvrII and XmaI restriction enzymes to
624 generate tub-DD-Myc-FER1^{FL}/sagCAT and in tub DD-YFP-TgNek1-2(MCS)/sagCAT [94]to
625 generate tub-DD-YFP-FER1^{FL}/sagCAT. FER1ΔTM constructs were generated by amplifying a
626 3' section without TM domain (primer pair 1651/1652; deletion of the C-terminal 21 aa) and
627 cloning the product in the FER1-FL plasmids using NheI and XmaI. The FER1 Ca^{2+}-binding
628 mutants in the C2D domain were generated by Q5 site directed mutagenesis kit (NEB) using
629 primers 4833/4834 to change positions A1622 and A1634 to C resulting in Asp codon 542 and
630 545 changes to Ala.

631 Plasmid tub-YFP-FER1(TM) encoding only the 31 most C-terminal aa of FER1
632 including the TM domain was cloned by PCR amplification using primer pair 4786/4788 and
633 cloned by Gibson assembly into BglII/AvrII digested tub-YFPYFP/sagCAT plasmid [46].
634 Plasmid tub-IMC3mCherry/DHFR was cloned by swapping IMC3mCherry from tub-
635 IMC3mCherry/sagCAT [95] with PmeI/AvrII into tub-YFPYFP(MCS)/DHFR [46].
636 To generate pmic3-MIC3-Cherry/DHFR 1.3 kb of promoter region together with 1.2 kb
637 of the ORF encoding genomic locus was PCR amplified from genomic DNA (primer pair
638 4864/4865) and Gibson assembled into PmeI and AvrII digested tub-mCherry$_2$/DHFR [96].
639
640 **Antiserum generation**
641 TgFER1 amino acids 669-877 including the diverse C2 domain DE were PCR amplified using
642 primers Ava-LIC-Fer1-F/R and fused to a 6xHis tag in plasmid pAVA0421 [97], expressed in
643 *Escherichia coli* BL21, purified by Ni-NTA chromatography (Invitrogen), and used to immunize
644 a guinea pig (Covance, Inc). Serum was affinity purified as described previously [98] against
645 recombinant His6-TgFER1.
646
647 **Live-cell microscopy**
648 For monitoring egress (P30-YFP and GCaMP3 expression), parasites were grown in hTERT
649 confluent 15 mm glass bottom cell culture dish (MatTek Corporation, cat #801002) for 30 hrs
650 and then induced with 2 µM Shield-1 for 90 min at 37ºC. Dishes were live-cell imaged on a
651 Zeiss Axiovert 200M inverted microscope for 15 min at 2 images per minute. To monitor DD-
652 YFP-FER1ΔTM accumulation a Leica TCS SP5 scanning confocal microscope with incubation
653 chamber in the Boston College Imaging Core in consultation with Bret Judson. Upon addition of
654 1 µM Shield-1 images were captured every 5 mins for 3 hrs. All images were acquired, analyzed
655 and adjusted using Leica, Volocity (Quorum Technologies) and/or ImageJ/FIJI software [99,
656 100].
657
658 **(Immuno-) fluorescence microscopy**
659 Indirect immunofluorescence assays were performed on intracellular parasites grown for 18 hrs
660 in 6-well plate containing coverslips confluent with HFF cells fixed with 100% methanol (unless
661 stated otherwise) using primary antisera as listed in Supplementary Table S3. Alexa 488 (A488)

662 or A594 conjugated goat α-mouse, α-rabbit, α-rat, or α-guinea pig were used as secondary
663 antibodies (1:500, Invitrogen). DNA was stained with 4',6-diamidino-2-phenylindole (DAPI).
664 For intracellular IFAs, parasites were allowed to invade and replicate for 24 h after which 1 μM
665 Shield-1 was applied for 18 hr (DD-Myc/YFP-FERΔTM) or 2 μM Shield-1 for 3 hr (DD-Myc-
666 FER^{FL}). Extracellular parasites grown ± Shield-1 for 18 hr were harvested by mechanical lysis
667 and captured on Poly-L-lysine coated coverslips. A Zeiss Axiovert 200 M wide-field
668 fluorescence microscope was used to collect images, which were deconvolved and adjusted for
669 phase contrast using Volocity software). SR- SIM was performed on intracellular parasites fixed
670 with 3.7% or 4% PFA in PBS and permeabilized with 0.25% or 0.5% TX-100 that were imaged
671 with a Zeiss ELYRA S.1 system in the Boston College Imaging Core in consultation with Bret
672 Judson. All images were acquired, analyzed and adjusted using ZEN software and standard
673 settings. Final image analyses were made with ImageJ/FIJI software [99, 100].
674
675 **Electron microscopy**
676 For ultrastructural observations of *T. gondii*-infected cells by thin-section transmission electron
677 microscopy (TEM), infected cells were fixed in 2.5% glutaraldehyde in 0.1 mM sodium
678 cacodylate (EMS) and processed as described [101]. Ultrathin sections of infected cells were
679 stained before examination with a Philips CM120 EM (Eindhoven, the Netherlands) under 80
680 kV. For immunoelectron microscopy (IEM) samples were prepared as described before [46].
681 Sections were immunolabeled with MIC2 MAb 6D10 in 1% fish skin gelatin and then with goat
682 anti-IgG antibodies, followed by 10-nm protein A-gold particles before examination with a
683 Philips CM120 electron microscope under 80 kV.
684
685 **Host cell invasion**
686 Extracellular parasites from 80% naturally lysed flask were induced with 2 μM Shield-1 for 90
687 min at 37ºC before they were allowed to invade HFF host cells for 10 min at 37ºC [7]. The
688 red/green invasion assay was performed as described [102] using Alexa594- and Alexa488-
689 conjugated SAG1 MAb T41E5. Three images were taken per biological replicate on an EVOS
690 FL (Life Technologies). The number of invaded versus uninvaded parasites were enumerated
691 manually for at least 300 parasites per counted sample.
692

693 **Secretagogue induced egress**

694 The egress assay was performed essentially as described previously [46]. Parasites were grown
695 in HFF monolayers for 30 h after which the phenotype was induced with 1 μM Shield-1 for 18
696 hrs. Egress was triggered with 1-3 μM A23187, 500 μM propranolol, 50-150 μM BIPPO (kindly
697 shared by Dr. Jeff Dvorin) 0.01-0.1% saponin or DMSO for 5 min at 37°C, followed by IFA
698 with IMC3 and GRA3 antisera. Egressed, permeabilized and intact vacuoles were counted [63].
699 100 vacuoles were counted for each experiment and three biological replicates were performed.
700

701 **Shield-1 induced egress**

702 Parasites were inoculated on HFF coverslips and allowed to grow for 30 hrs and then induced
703 with either 1 μM Shield-1 for 2 hrs or 1 μM calcium ionophore A23187 for 5 min as a control,
704 prior to fixation with 100% methanol and IFA staining using MAb 9E10 cMyc and rabbit αMIC8
705 (antisera details in Supplementary Table S1). DNA was stained with 4',6-diamidino-2-
706 phenylindole (DAPI). The number of intact vacuoles per 20 fields was enumerated.
707

708 **Combined invasion-egress Assay**

709 Parasites were grown for 36 hours, mechanically lysed in standard ED1 parasite medium and
710 allowed to invade coverslips coated in an HFF monolayer for 1 hr. All unattached parasites were
711 then washed off with a PBS and coverslips were incubated in 1 μM Shield-1 or vehicle control
712 for an additional 2 hrs. Coverslips were then fixed with PFA and IFA was performed as
713 described for a typical red-green invasion assay.
714

715 **Shield-1 induced microneme secretion**

716 Parasites were grown for 30 hrs in a T25 hTERT containing flask. Flasks were washed once with
717 PBS and once with Endo buffer (20 mM Tris-H_2SO_4 pH 8.2, 44.7 mM K_2SO_4, 106 mM sucrose,
718 3.5 mg/ml BSA,10 mM $MgSO_4$) [62]. Cells were scraped and parasites mechanically released.
719 Parasites pellets were re-suspended in Endo buffer and treated with either 1 μM Shield-1 for 2
720 hrs or A23187 for 5 min prior to processing. All other secretion steps are as previously stated.
721 Supernatants were processed for western blot.
722

723 **Microneme secretion by Western blotting**

724 Microneme secretion by western blot was performed as published [103]. Freshly lysed parasites
725 were resuspended in DMEM/FBS and transferred to a 96-well polystyrene round-bottom plate
726 (CELLTREAT Scientific Products). Secretion was induced by 1-3 μM A23187, 500 μM
727 propranolol, 1% ethanol or DMSO for 5 min at 37°C. Constitutive microneme secretion was
728 assessed by incubation without secretagogue at 37°C for 60 min. Supernatants were probed by
729 western blot using 6D10 MIC2 MAb and TG17.43 GRA1 MAb and HRP conjugated secondary
730 antiserum. Signals were quantified using a densitometer.
731
732 **Microneme secretion by IFA**
733 IFA on parasites exposed to a host cell monolayer was performed as reported [46]. Parasites
734 were resuspended in Endo buffer and spun onto HFF cells in a 6-well plate at 28*g, 5 min, RT
735 and allowed to settle for 20 min at 37°C. Secretion was induced by replacing the buffer with 3%
736 FBS in DMEM and 10 mM HEPES (pH 7.2) and incubation at 37°C for 5 min. PBS-washed
737 coverslips were fixed with 4% formaldehyde and 0.02% glutaraldehyde, and subjected to IFA
738 with anti-Mic3, -Mic5, -Mic8 or Mic10 in the presence of 0.02% saponin.
739
740 **Gliding motility trail assay**
741 Trail assays were performed as previously described [22]. Parasites were induced with 1 μM
742 Shield-1 for 18 hr, mechanically released, resuspended in ED1 with 1 μM Shield-1 and
743 incubated on poly-L-lysine coated coverslips for 15 min at 37°C. Parasites were fixed with 4%
744 formaldehyde and 0.02% glutaraldehyde and stained with DG52 SAG1 MAb (64) to visualize
745 trails.
746
747 **Statistics.**
748 Student's paired t test and one-way analysis of variance (ANOVA) using post hoc Bonferroni
749 correction were performed.
750
751
752 **Acknowledgements**
753 We thank Bret Judson and Dr. Patrick Autissier of the Boston College Imaging and Flow
754 Cytometry Cores, respectively, for infrastructure and support, Dr. Sander Groffen for assistance

755 with molecular modeling, Emily Stoneburner, Natalie Sandlin, and Elizabeth Gray for technical
756 support, Drs. Gustavo Arrizabalaga, Peter Bradley, Vern Carruthers, Iain Cheeseman, Jean-
757 François Dubremetz, Wassim Daher, Jeff Dvorin, Maryse Lebrun, Sebastian Lourido, Sabrina
758 Marion, Silvia Moreno, Naomi Morrissette, Jeroen Saeij, David Sibley, Dominique Soldati-
759 Favre, and Gary Ward for sharing reagents.
760 This study was supported by National Science Foundation (NSF) Major Research
761 Instrumentation grant 1626072, National Institutes of Health grants AI108251 (B.I.C.),
762 AI060767 (I.C.), AI122042 (M.-J.G), AI099658 (M.-J.G.), and AI122923 (M.-J.G.), and
763 American Cancer Society grant RSG-12-175-01-MPC (M.-J.G.).
764

765 **Author contributions**

766 DNAT performed all experiments on the DD-[Myc/YFP]-FER1ΔTM parasites, imaging of the
767 DD-Myc-FER1^{FL} line, all time lapse and super resolution microscopy and generated and
768 assessed the Asp-Ala mutants, AAD performed all functional studies on the DD-Myc-FER1^{FL}
769 parasites, IC performed all electron microscopy studies, BIC cloned FER1 cDNA, established
770 the overexpression plasmids and assessed the initial phenotype, DNAT, AAD and MJG designed
771 the experiments and interpreted the data, MJG wrote the manuscript and all authors reviewed and
772 edited the manuscript.
773

774 **Conflict of interest**

775 The authors declare no conflict of interest.
776
777

778 **References**
779

780 1. Blader, I.J., B.I. Coleman, C.T. Chen, and M.J. Gubbels, 2015. *Lytic Cycle of*
781 *Toxoplasma gondii: 15 Years Later.* Annu Rev Microbiol, 69: 463-85.
782 2. Carruthers, V.B. and F.M. Tomley, 2008. *Microneme proteins in apicomplexans.* Subcell
783 Biochem, 47: 33-45.
784 3. Sheiner, L., J.M. Santos, N. Klages, F. Parussini, N. Jemmely, N. Friedrich, G.E. Ward,
785 and D. Soldati-Favre, 2010. *Toxoplasma gondii transmembrane microneme proteins and*
786 *their modular design.* Mol Microbiol.
787 4. Kafsack, B.F., J.D. Pena, I. Coppens, S. Ravindran, J.C. Boothroyd, and V.B. Carruthers,
788 2009. *Rapid membrane disruption by a perforin-like protein facilitates parasite exit from*
789 *host cells.* Science, 323: 530-3.

790 5. Roiko, M.S., N. Svezhova, and V.B. Carruthers, 2014. *Acidification Activates*
791 *Toxoplasma gondii Motility and Egress by Enhancing Protein Secretion and Cytolytic*
792 *Activity.* PLoS Pathog, 10: e1004488.
793 6. Bullen, H.E., H. Bisio, and D. Soldati-Favre, 2019. *The triumvirate of signaling*
794 *molecules controlling Toxoplasma microneme exocytosis: Cyclic GMP, calcium, and*
795 *phosphatidic acid.* PLoS Pathog, 15: e1007670.
796 7. Uboldi, A.D., M.L. Wilde, E.A. McRae, R.J. Stewart, L.F. Dagley, L. Yang, N.J. Katris,
797 S.V. Hapuarachchi, M.J. Coffey, A.M. Lehane, C.Y. Botte, R.F. Waller, A.I. Webb, M.J.
798 McConville, and C.J. Tonkin, 2018. *Protein kinase A negatively regulates Ca2+*
799 *signalling in Toxoplasma gondii.* PLoS Biol, 16: e2005642.
800 8. Leung, J.M., Y. He, F. Zhang, Y.C. Hwang, E. Nagayasu, J. Liu, J.M. Murray, and K.
801 Hu, 2017. *Stability and function of a putative microtubule-organizing center in the*
802 *human parasite Toxoplasma gondii.* Mol Biol Cell, 28: 1361-1378.
803 9. Kremer, K., D. Kamin, E. Rittweger, J. Wilkes, H. Flammer, S. Mahler, J. Heng, C.J.
804 Tonkin, G. Langsley, S.W. Hell, V.B. Carruthers, D.J. Ferguson, and M. Meissner, 2013.
805 *An overexpression screen of Toxoplasma gondii Rab-GTPases reveals distinct transport*
806 *routes to the micronemes.* PLoS Pathog, 9: e1003213.
807 10. Jacot, D., N. Tosetti, I. Pires, J. Stock, A. Graindorge, Y.F. Hung, H. Han, R. Tewari, I.
808 Kursula, and D. Soldati-Favre, 2016. *An Apicomplexan Actin-Binding Protein Serves as a*
809 *Connector and Lipid Sensor to Coordinate Motility and Invasion.* Cell Host Microbe, 20:
810 731-743.
811 11. Sakura, T., F. Sindikubwabo, L.K. Oesterlin, H. Bousquet, C. Slomianny, M.A. Hakimi,
812 G. Langsley, and S. Tomavo, 2016. *A Critical Role for Toxoplasma gondii Vacuolar*
813 *Protein Sorting VPS9 in Secretory Organelle Biogenesis and Host Infection.* Scientific
814 Reports, 6.
815 12. Paredes-Santos, T.C., W. de Souza, and M. Attias, 2012. *Dynamics and 3D organization*
816 *of secretory organelles of Toxoplasma gondii.* Journal of structural biology, 177: 420-30.
817 13. Saha, S., B.I. Coleman, R. Dubey, I.J. Blader, and M.J. Gubbels, 2017. *Two*
818 *Phosphoglucomutase Paralogs Facilitate Ionophore-Triggered Secretion of the*
819 *Toxoplasma Micronemes.* mSphere, 2.
820 14. Venugopal, K. and S. Marion, 2018. *Secretory organelle trafficking in Toxoplasma*
821 *gondii: A long story for a short travel.* Int J Med Microbiol, 308: 751-760.
822 15. Sangare, L.O., T.D. Alayi, B. Westermann, A. Hovasse, F. Sindikubwabo, I. Callebaut,
823 E. Werkmeister, F. Lafont, C. Slomianny, M.A. Hakimi, A. Van Dorsselaer, C.
824 Schaeffer-Reiss, and S. Tomavo, 2016. *Unconventional endosome-like compartment and*
825 *retromer complex in Toxoplasma gondii govern parasite integrity and host infection.* Nat
826 Commun, 7: 11191.
827 16. Tomavo, S., C. Slomianny, M. Meissner, and V.B. Carruthers, 2013. *Protein trafficking*
828 *through the endosomal system prepares intracellular parasites for a home invasion.*
829 PLoS Pathog, 9: e1003629.
830 17. Thornton, L.B., P. Teehan, K. Floyd, C. Cochrane, A. Bergmann, B. Riegel, A.J. Stasic,
831 M. Di Cristina, S.N.J. Moreno, P.D. Roepe, and Z. Dou, 2019. *An ortholog of*
832 *Plasmodium falciparum chloroquine resistance transporter (PfCRT) plays a key role in*
833 *maintaining the integrity of the endolysosomal system in Toxoplasma gondii to facilitate*
834 *host invasion.* PLoS Pathog, 15: e1007775.

835 18. Dubois, D.J. and D. Soldati-Favre, 2019. *Biogenesis and secretion of micronemes in*
836 *Toxoplasma gondii.* Cell Microbiol, 21: e13018.
837 19. McGovern, O.L., Y. Rivera-Cuevas, G. Kannan, A.J. Narwold, and V.B. Carruthers,
838 2018. *Intersection of endocytic and exocytic systems in Toxoplasma gondii.* Traffic, 19:
839 336-353.
840 20. Stasic, A.J., N.M. Chasen, E.J. Dykes, S.A. Vella, B. Asady, V.J. Starai, and S.N.J.
841 Moreno, 2019. *The Toxoplasma Vacuolar H(+)-ATPase Regulates Intracellular pH and*
842 *Impacts the Maturation of Essential Secretory Proteins.* Cell Rep, 27: 2132-2146 e7.
843 21. Sloves, P.J., S. Delhaye, T. Mouveaux, E. Werkmeister, C. Slomianny, A. Hovasse, T.
844 Dilezitoko Alayi, I. Callebaut, R.Y. Gaji, C. Schaeffer-Reiss, A. Van Dorsselear, V.B.
845 Carruthers, and S. Tomavo, 2012. *Toxoplasma sortilin-like receptor regulates protein*
846 *transport and is essential for apical secretory organelle biogenesis and host infection.*
847 Cell Host Microbe, 11: 515-27.
848 22. Morlon-Guyot, J., S. Pastore, L. Berry, M. Lebrun, and W. Daher, 2015. *Toxoplasma*
849 *gondii Vps11, a subunit of HOPS and CORVET tethering complexes, is essential for the*
850 *biogenesis of secretory organelles.* Cellular Microbiology.
851 23. Venugopal, K., E. Werkmeister, N. Barois, J.M. Saliou, A. Poncet, L. Huot, F.
852 Sindikubwabo, M.A. Hakimi, G. Langsley, F. Lafont, and S. Marion, 2017. *Dual role of*
853 *the Toxoplasma gondii clathrin adaptor AP1 in the sorting of rhoptry and microneme*
854 *proteins and in parasite division.* PLoS Pathog, 13: e1006331.
855 24. Bradley, P.J. and J.C. Boothroyd, 2001. *The pro region of Toxoplasma ROP1 is a*
856 *rhoptry-targeting signal.* Int J Parasitol, 31: 1177-86.
857 25. Bradley, P.J., N. Li, and J.C. Boothroyd, 2004. *A GFP-based motif-trap reveals a novel*
858 *mechanism of targeting for the Toxoplasma ROP4 protein.* Mol Biochem Parasitol, 137:
859 111-20.
860 26. Lentini, G., D.J. Dubois, B. Maco, D. Soldati-Favre, and K. Frenal, 2019. *The roles of*
861 *Centrin 2 and Dynein Light Chain 8a in apical secretory organelles discharge of*
862 *Toxoplasma gondii.* Traffic.
863 27. Farrell, A., S. Thirugnanam, A. Lorestani, J.D. Dvorin, K.P. Eidell, D.J. Ferguson, B.R.
864 Anderson-White, M.T. Duraisingh, G.T. Marth, and M.J. Gubbels, 2012. *A DOC2*
865 *protein identified by mutational profiling is essential for apicomplexan parasite*
866 *exocytosis.* Science, 335: 218-21.
867 28. Bullen, H.E., Y. Jia, Y. Yamaryo-Botte, H. Bisio, O. Zhang, N.K. Jemelin, J.B. Marq, V.
868 Carruthers, C.Y. Botte, and D. Soldati-Favre, 2016. *Phosphatidic Acid-Mediated*
869 *Signaling Regulates Microneme Secretion in Toxoplasma.* Cell Host Microbe, 19: 349-
870 60.
871 29. Venugopal, K., S. Chehade, E. Werkmeister, N. Barois, J. Periz, F. Lafont, I. Tardieux, J.
872 Khalife, G. Langsley, M. Meissner, and S. Marion, 2019. *Rab11A regulates the*
873 *constitutive secretory pathway during Toxoplasma gondii invasion of host cells and*
874 *parasite replication.* bioRxiv.
875 30. Bullen, H.E. and D. Soldati-Favre, 2016. *A central role for phosphatidic acid as a lipid*
876 *mediator of regulated exocytosis in apicomplexa.* FEBS Lett, 590: 2469-81.
877 31. Gras, S., E. Jimenez-Ruiz, C.M. Klinger, K. Schneider, A. Klingl, L. Lemgruber, and M.
878 Meissner, 2019. *An endocytic-secretory cycle participates in Toxoplasma gondii in*
879 *motility.* PLoS Biol, 17: e3000060.

880 32. Periz, J., M. Del Rosario, A. McStea, S. Gras, C. Loney, L. Wang, M.L. Martin-
881 Fernandez, and M. Meissner, 2019. *A highly dynamic F-actin network regulates*
882 *transport and recycling of micronemes in Toxoplasma gondii vacuoles.* Nat Commun,
883 10: 4183.
884 33. Martens, S. and H.T. McMahon, 2008. *Mechanisms of membrane fusion: disparate*
885 *players and common principles.* Nat Rev Mol Cell Biol, 9: 543-56.
886 34. Martens, S., 2010. *Role of C2 domain proteins during synaptic vesicle exocytosis.*
887 Biochem Soc Trans, 38: 213-6.
888 35. Corbalan-Garcia, S. and J.C. Gomez-Fernandez, 2014. *Signaling through C2 domains:*
889 *more than one lipid target.* Biochim Biophys Acta, 1838: 1536-47.
890 36. Striegel, A.R., L.M. Biela, C.S. Evans, Z. Wang, J.B. Delehoy, R.B. Sutton, E.R.
891 Chapman, and N.E. Reist, 2012. *Calcium binding by synaptotagmin's C2A domain is an*
892 *essential element of the electrostatic switch that triggers synchronous synaptic*
893 *transmission.* J Neurosci, 32: 1253-60.
894 37. Davis, D.B., K.R. Doherty, A.J. Delmonte, and E.M. McNally, 2002. *Calcium-sensitive*
895 *phospholipid binding properties of normal and mutant ferlin C2 domains.* J Biol Chem,
896 277: 22883-8.
897 38. Verdaguer, N., S. Corbalan-Garcia, W.F. Ochoa, I. Fita, and J.C. Gomez-Fernandez,
898 1999. *Ca(2+) bridges the C2 membrane-binding domain of protein kinase Calpha*
899 *directly to phosphatidylserine.* EMBO J, 18: 6329-38.
900 39. Chapman, E.R. and A.F. Davis, 1998. *Direct interaction of a Ca2+-binding loop of*
901 *synaptotagmin with lipid bilayers.* J Biol Chem, 273: 13995-4001.
902 40. Lek, A., F.J. Evesson, R.B. Sutton, K.N. North, and S.T. Cooper, 2012. *Ferlins:*
903 *regulators of vesicle fusion for auditory neurotransmission, receptor trafficking and*
904 *membrane repair.* Traffic, 13: 185-94.
905 41. Redpath, G.M., R.A. Sophocleous, L. Turnbull, C.B. Whitchurch, and S.T. Cooper, 2016.
906 *Ferlins Show Tissue-Specific Expression and Segregate as Plasma Membrane/Late*
907 *Endosomal or Trans-Golgi/Recycling Ferlins.* Traffic, 17: 245-66.
908 42. Roux, I., S. Safieddine, R. Nouvian, M. Grati, M.C. Simmler, A. Bahloul, I. Perfettini, M.
909 Le Gall, P. Rostaing, G. Hamard, A. Triller, P. Avan, T. Moser, and C. Petit, 2006.
910 *Otoferlin, defective in a human deafness form, is essential for exocytosis at the auditory*
911 *ribbon synapse.* Cell, 127: 277-89.
912 43. Pangrsic, T., E. Reisinger, and T. Moser, 2012. *Otoferlin: a multi-C2 domain protein*
913 *essential for hearing.* Trends in neurosciences, 35: 671-80.
914 44. Hams, N., M. Padmanarayana, W. Qiu, and C.P. Johnson, 2017. *Otoferlin is a multivalent*
915 *calcium-sensitive scaffold linking SNAREs and calcium channels.* Proc Natl Acad Sci U S
916 A, 114: 8023-8028.
917 45. Michalski, N., J.D. Goutman, S.M. Auclair, J. Boutet de Monvel, M. Tertrais, A. Emptoz,
918 A. Parrin, S. Nouaille, M. Guillon, M. Sachse, D. Ciric, A. Bahloul, J.P. Hardelin, R.B.
919 Sutton, P. Avan, S.S. Krishnakumar, J.E. Rothman, D. Dulon, S. Safieddine, and C. Petit,
920 2017. *Otoferlin acts as a Ca(2+) sensor for vesicle fusion and vesicle pool replenishment*
921 *at auditory hair cell ribbon synapses.* Elife, 6.
922 46. Coleman, B.I., S. Saha, S. Sato, K. Engelberg, D.J.P. Ferguson, I. Coppens, M. Lodoen,
923 and M.-J. Gubbels, 2018. *A member of the ferlin calcium sensor family is essential for*
924 *Toxoplasma gondii rhoptry secretion.* mBio, 9: e01510-18.

925 47. Obrova, K., M. Cyrklaff, R. Frank, G.R. Mair, and A.K. Mueller, 2018. *Transmission of*
926 *the malaria parasite requires ferlin for gamete egress from the red blood cell.* Cell
927 Microbiol: e12999.
928 48. Sidik, S.M., D. Huet, S.M. Ganesan, M.H. Huynh, T. Wang, A.S. Nasamu, P. Thiru, J.P.
929 Saeij, V.B. Carruthers, J.C. Niles, and S. Lourido, 2016. *A Genome-wide CRISPR Screen*
930 *in Toxoplasma Identifies Essential Apicomplexan Genes.* Cell, 166: 1423-1435 e12.
931 49. Padgett, L.R., G. Arrizabalaga, and W.J. Sullivan, Jr., 2017. *Targeting of tail-anchored*
932 *membrane proteins to subcellular organelles in Toxoplasma gondii.* Traffic, 18: 149-
933 158.
934 50. Breinich, M.S., D.J. Ferguson, B.J. Foth, G.G. van Dooren, M. Lebrun, D.V. Quon, B.
935 Striepen, P.J. Bradley, F. Frischknecht, V.B. Carruthers, and M. Meissner, 2009. *A*
936 *Dynamin Is Required for the Biogenesis of Secretory Organelles in Toxoplasma gondii.*
937 Curr Biol, 19: 277-86.
938 51. Miranda, K., D.A. Pace, R. Cintron, J.C. Rodrigues, J. Fang, A. Smith, P. Rohloff, E.
939 Coelho, F. de Haas, W. de Souza, I. Coppens, L.D. Sibley, and S.N. Moreno, 2010.
940 *Characterization of a novel organelle in Toxoplasma gondii with similar composition*
941 *and function to the plant vacuole.* Mol Microbiol, 76: 1358-75.
942 52. Drozdowicz, Y.M., M. Shaw, M. Nishi, B. Striepen, H.A. Liwinski, D.S. Roos, and P.A.
943 Rea, 2003. *Isolation and characterization of TgVP1, a type I vacuolar H+-translocating*
944 *pyrophosphatase from Toxoplasma gondii. The dynamics of its subcellular localization*
945 *and the cellular effects of a diphosphonate inhibitor.* J Biol Chem, 278: 1075-85.
946 53. Luo, S., F.A. Ruiz, and S.N. Moreno, 2005. *The acidocalcisome Ca2+-ATPase (TgA1) of*
947 *Toxoplasma gondii is required for polyphosphate storage, intracellular calcium*
948 *homeostasis and virulence.* Mol Microbiol, 55: 1034-45.
949 54. Francia, M.E., S. Wicher, D.A. Pace, J. Sullivan, S.N. Moreno, and G. Arrizabalaga,
950 2011. *A Toxoplasma gondii protein with homology to intracellular type Na(+)/H(+)*
951 *exchangers is important for osmoregulation and invasion.* Exp Cell Res.
952 55. Herm-Gotz, A., C. Agop-Nersesian, S. Munter, J.S. Grimley, T.J. Wandless, F.
953 Frischknecht, and M. Meissner, 2007. *Rapid control of protein level in the apicomplexan*
954 *Toxoplasma gondii.* Nat Methods, 4: 1003-5.
955 56. Garrison, E., M. Treeck, E. Ehret, H. Butz, T. Garbuz, B.P. Oswald, M. Settles, J.
956 Boothroyd, and G. Arrizabalaga, 2012. *A forward genetic screen reveals that calcium-*
957 *dependent protein kinase 3 regulates egress in Toxoplasma.* PLoS Pathog, 8: e1003049.
958 57. Lourido, S., K. Tang, and L.D. Sibley, 2012. *Distinct signalling pathways control*
959 *Toxoplasma egress and host-cell invasion.* Embo J, 31: 4524-34.
960 58. McCoy, J.M., L. Whitehead, G.G. van Dooren, and C.J. Tonkin, 2012. *TgCDPK3*
961 *Regulates Calcium-Dependent Egress of Toxoplasma gondii from Host Cells.* PLoS
962 Pathog, 8: e1003066.
963 59. Parussini, F., I. Coppens, P.P. Shah, S.L. Diamond, and V.B. Carruthers, 2010. *Cathepsin*
964 *L occupies a vacuolar compartment and is a protein maturase within the endo/exocytic*
965 *system of Toxoplasma gondii.* Mol Microbiol, 76: 1340-57.
966 60. Brydges, S.D., J.M. Harper, F. Parussini, I. Coppens, and V.B. Carruthers, 2008. *A*
967 *transient forward-targeting element for microneme-regulated secretion in Toxoplasma*
968 *gondii.* Biology of the Cell, 100: 253-264.
969 61. Nishi, M., K. Hu, J.M. Murray, and D.S. Roos, 2008. *Organellar dynamics during the*
970 *cell cycle of Toxoplasma gondii.* J Cell Sci, 121: 1559-1568.

971 62. Endo, T. and K. Yagita, 1990. *Effect of extracellular ions on motility and cell entry in*
972 *Toxoplasma gondii.* J Protozool, 37: 133-8.
973 63. Bisio, H., M. Lunghi, M. Brochet, and D. Soldati-Favre, 2019. *Phosphatidic acid governs*
974 *natural egress in Toxoplasma gondii via a guanylate cyclase receptor platform.* Nat
975 Microbiol, 4: 420-428.
976 64. Kafsack, B.F., C. Beckers, and V.B. Carruthers, 2004. *Synchronous invasion of host cells*
977 *by Toxoplasma gondii.* Mol Biochem Parasitol, 136: 309-11.
978 65. Vogl, C., I. Panou, G. Yamanbaeva, C. Wichmann, S.J. Mangosing, F. Vilardi, A.A.
979 Indzhykulian, T. Pangrsic, R. Santarelli, M. Rodriguez-Ballesteros, T. Weber, S. Jung, E.
980 Cardenas, X. Wu, S.M. Wojcik, K.Y. Kwan, I. Del Castillo, B. Schwappach, N. Strenzke,
981 D.P. Corey, S.Y. Lin, and T. Moser, 2016. *Tryptophan-rich basic protein (WRB)*
982 *mediates insertion of the tail-anchored protein otoferlin and is required for hair cell*
983 *exocytosis and hearing.* EMBO J, 35: 2536-2552.
984 66. Kaeser, P.S. and W.G. Regehr, 2014. *Molecular mechanisms for synchronous,*
985 *asynchronous, and spontaneous neurotransmitter release.* Annu Rev Physiol, 76: 333-
986 63.
987 67. Kaeser, P.S. and W.G. Regehr, 2017. *The readily releasable pool of synaptic vesicles.*
988 Curr Opin Neurobiol, 43: 63-70.
989 68. Meese, S., A.P. Cepeda, F. Gahlen, C.M. Adams, R. Ficner, A.J. Ricci, S. Heller, E.
990 Reisinger, and M. Herget, 2017. *Activity-Dependent Phosphorylation by CaMKIIdelta*
991 *Alters the Ca(2+) Affinity of the Multi-C2-Domain Protein Otoferlin.* Front Synaptic
992 Neurosci, 9: 13.
993 69. Pangrsic, T., L. Lasarow, K. Reuter, H. Takago, M. Schwander, D. Riedel, T. Frank,
994 L.M. Tarantino, J.S. Bailey, N. Strenzke, N. Brose, U. Muller, E. Reisinger, and T.
995 Moser, 2010. *Hearing requires otoferlin-dependent efficient replenishment of synaptic*
996 *vesicles in hair cells.* Nat Neurosci, 13: 869-76.
997 70. Heidrych, P., U. Zimmermann, S. Kuhn, C. Franz, J. Engel, S.V. Duncker, B. Hirt, C.M.
998 Pusch, P. Ruth, M. Pfister, W. Marcotti, N. Blin, and M. Knipper, 2009. *Otoferlin*
999 *interacts with myosin VI: implications for maintenance of the basolateral synaptic*
1000 *structure of the inner hair cell.* Hum Mol Genet, 18: 2779-90.
1001 71. Ramakrishnan, N.A., M.J. Drescher, B.J. Morley, P.M. Kelley, and D.G. Drescher, 2014.
1002 *Calcium regulates molecular interactions of otoferlin with soluble NSF attachment*
1003 *protein receptor (SNARE) proteins required for hair cell exocytosis.* J Biol Chem, 289:
1004 8750-66.
1005 72. Johnson, C.P. and E.R. Chapman, 2010. *Otoferlin is a calcium sensor that directly*
1006 *regulates SNARE-mediated membrane fusion.* J Cell Biol, 191: 187-97.
1007 73. Lourido, S., J. Shuman, C. Zhang, K.M. Shokat, R. Hui, and L.D. Sibley, 2010. *Calcium-*
1008 *dependent protein kinase 1 is an essential regulator of exocytosis in Toxoplasma.* Nature,
1009 465: 359-62.
1010 74. Donald, R.G. and P.A. Liberator, 2002. *Molecular characterization of a coccidian*
1011 *parasite cGMP dependent protein kinase.* Mol Biochem Parasitol, 120: 165-75.
1012 75. Jia, Y., J.B. Marq, H. Bisio, D. Jacot, C. Mueller, L. Yu, J. Choudhary, M. Brochet, and
1013 D. Soldati-Favre, 2017. *Crosstalk between PKA and PKG controls pH-dependent host*
1014 *cell egress of Toxoplasma gondii.* EMBO J.

1015 76. Evans, C.S., Z. He, H. Bai, X. Lou, P. Jeggle, R.B. Sutton, J.M. Edwardson, and E.R.
1016 Chapman, 2016. *Functional analysis of the interface between the tandem C2 domains of*
1017 *synaptotagmin-1.* Mol Biol Cell, 27: 979-89.
1018 77. Shin, O.H., 2014. *Exocytosis and synaptic vesicle fusion.* Comprehensive Physiology, 4:
1019 149-175.
1020 78. Luo, S., M. Vieira, J. Graves, L. Zhong, and S.N. Moreno, 2001. *A plasma membrane-*
1021 *type Ca(2+)-ATPase co-localizes with a vacuolar H(+)-pyrophosphatase to*
1022 *acidocalcisomes of Toxoplasma gondii.* EMBO J, 20: 55-64.
1023 79. Morel, N. and S. Poea-Guyon, 2015. *The membrane domain of vacuolar H(+)ATPase: a*
1024 *crucial player in neurotransmitter exocytotic release.* Cell Mol Life Sci, 72: 2561-73.
1025 80. Morel, N., J.C. Dedieu, and J.M. Philippe, 2003. *Specific sorting of the a1 isoform of the*
1026 *V-H+ATPase a subunit to nerve terminals where it associates with both synaptic vesicles*
1027 *and the presynaptic plasma membrane.* J Cell Sci, 116: 4751-62.
1028 81. Rorsman, P. and E. Renstrom, 2003. *Insulin granule dynamics in pancreatic beta cells.*
1029 Diabetologia, 46: 1029-45.
1030 82. Barg, S., P. Huang, L. Eliasson, D.J. Nelson, S. Obermuller, P. Rorsman, F. Thevenod,
1031 and E. Renstrom, 2001. *Priming of insulin granules for exocytosis by granular Cl(-)*
1032 *uptake and acidification.* J Cell Sci, 114: 2145-54.
1033 83. Poea-Guyon, S., M.R. Ammar, M. Erard, M. Amar, A.W. Moreau, P. Fossier, V. Gleize,
1034 N. Vitale, and N. Morel, 2013. *The V-ATPase membrane domain is a sensor of granular*
1035 *pH that controls the exocytotic machinery.* J Cell Biol, 203: 283-98.
1036 84. Wang, D. and P.R. Hiesinger, 2013. *The vesicular ATPase: a missing link between*
1037 *acidification and exocytosis.* J Cell Biol, 203: 171-3.
1038 85. Andenmatten, N., S. Egarter, A.J. Jackson, N. Jullien, J.P. Herman, and M. Meissner,
1039 2012. *Conditional genome engineering in Toxoplasma gondii uncovers alternative*
1040 *invasion mechanisms.* Nat Methods, 10: 125-7.
1041 86. Agop-Nersesian, C., B. Naissant, F. Ben Rached, M. Rauch, A. Kretzschmar, S.
1042 Thiberge, R. Menard, D.J. Ferguson, M. Meissner, and G. Langsley, 2009. *Rab11A-*
1043 *controlled assembly of the inner membrane complex is required for completion of*
1044 *apicomplexan cytokinesis.* PLoS Pathog, 5: e1000270.
1045 87. Leung, J.M., J. Liu, L.A. Wetzel, and K. Hu, 2019. *Centrin2 from the human parasite*
1046 *Toxoplasma gondii is required for its invasion and intracellular replication.* J Cell Sci,
1047 132.
1048 88. Ebrahimzadeh, Z., A. Mukherjee, M.E. Crochetiere, A. Sergerie, S. Amiar, L.A.
1049 Thompson, D. Gagnon, D. Gaumond, R.V. Stahelin, J.B. Dacks, and D. Richard, 2019. *A*
1050 *pan-apicomplexan phosphoinositide-binding protein acts in malarial microneme*
1051 *exocytosis.* EMBO Rep, 20.
1052 89. Nouvian, R., J. Neef, A.V. Bulankina, E. Reisinger, T. Pangrsic, T. Frank, S. Sikorra, N.
1053 Brose, T. Binz, and T. Moser, 2011. *Exocytosis at the hair cell ribbon synapse apparently*
1054 *operates without neuronal SNARE proteins.* Nat Neurosci, 14: 411-3.
1055 90. Meriney, S.D., J.A. Umbach, and C.B. Gundersen, 2014. *Fast, Ca2+-dependent*
1056 *exocytosis at nerve terminals: shortcomings of SNARE-based models.* Prog Neurobiol,
1057 121: 55-90.
1058 91. Liu, Y., Y. Sugiura, T.C. Sudhof, and W. Lin, 2019. *Ablation of All Synaptobrevin*
1059 *vSNAREs Blocks Evoked But Not Spontaneous Neurotransmitter Release at*
1060 *Neuromuscular Synapses.* J Neurosci, 39: 6049-6066.

1061 92. Lek, A., M. Lek, K.N. North, and S.T. Cooper, 2010. *Phylogenetic analysis of ferlin*
1062 *genes reveals ancient eukaryotic origins.* BMC Evol Biol, 10: 231.
1063 93. Roos, D.S., R.G. Donald, N.S. Morrissette, and A.L. Moulton, 1994. *Molecular tools for*
1064 *genetic dissection of the protozoan parasite Toxoplasma gondii.* Methods Cell Biol, 45:
1065 27-63.
1066 94. Chen, C.T. and M.J. Gubbels, 2013. *The Toxoplasma gondii centrosome is the platform*
1067 *for internal daughter budding as revealed by a Nek1 kinase mutant.* J Cell Sci, 126:
1068 3344-55.
1069 95. Anderson-White, B.R., F.D. Ivey, K. Cheng, T. Szatanek, A. Lorestani, C.J. Beckers, D.J.
1070 Ferguson, N. Sahoo, and M.J. Gubbels, 2011. *A family of intermediate filament-like*
1071 *proteins is sequentially assembled into the cytoskeleton of Toxoplasma gondii.* Cell
1072 Microbiol, 13: 18-31.
1073 96. Schaeffer, M., S.J. Han, T. Chtanova, G.G. van Dooren, P. Herzmark, Y. Chen, B.
1074 Roysam, B. Striepen, and E.A. Robey, 2009. *Dynamic imaging of T cell-parasite*
1075 *interactions in the brains of mice chronically infected with Toxoplasma gondii.* J
1076 Immunol, 182: 6379-93.
1077 97. Alexandrov, A., M. Vignali, D.J. LaCount, E. Quartley, C. de Vries, D. De Rosa, J.
1078 Babulski, S.F. Mitchell, L.W. Schoenfeld, S. Fields, W.G. Hol, M.E. Dumont, E.M.
1079 Phizicky, and E.J. Grayhack, 2004. *A facile method for high-throughput co-expression of*
1080 *protein pairs.* Mol Cell Proteomics, 3: 934-8.
1081 98. Gubbels, M.J., S. Vaishnava, N. Boot, J.F. Dubremetz, and B. Striepen, 2006. *A MORN-*
1082 *repeat protein is a dynamic component of the Toxoplasma gondii cell division apparatus.*
1083 J Cell Sci, 119: 2236-45.
1084 99. Abramoff, M.D., P.J. Magalhaes, and S.J. Ram, 2004. *Image Processing with ImageJ.*
1085 Biophotonics International, 11: 36-42.
1086 100. Schindelin, J., I. Arganda-Carreras, E. Frise, V. Kaynig, M. Longair, T. Pietzsch, S.
1087 Preibisch, C. Rueden, S. Saalfeld, B. Schmid, J.Y. Tinevez, D.J. White, V. Hartenstein,
1088 K. Eliceiri, P. Tomancak, and A. Cardona, 2012. *Fiji: an open-source platform for*
1089 *biological-image analysis.* Nat Methods, 9: 676-82.
1090 101. Coppens, I. and K.A. Joiner, 2003. *Host but not parasite cholesterol controls Toxoplasma*
1091 *cell entry by modulating organelle discharge.* Mol Biol Cell, 14: 3804-20.
1092 102. Carey, K.L., N.J. Westwood, T.J. Mitchison, and G.E. Ward, 2004. *A small-molecule*
1093 *approach to studying invasive mechanisms of Toxoplasma gondii.* Proc Natl Acad Sci U
1094 S A, 101: 7433-8.
1095 103. Carruthers, V.B. and L.D. Sibley, 1999. *Mobilization of intracellular calcium stimulates*
1096 *microneme discharge in Toxoplasma gondii.* Mol Microbiol, 31: 421-8.
1097 104. Jimenez, J.L. and R. Bashir, 2007. *In silico functional and structural characterisation of*
1098 *ferlin proteins by mapping disease-causing mutations and evolutionary information onto*
1099 *three-dimensional models of their C2 domains.* J Neurol Sci, 260: 114-23.
1100 105. Hartmann, J., K. Hu, C.Y. He, L. Pelletier, D.S. Roos, and G. Warren, 2006. *Golgi and*
1101 *centrosome cycles in Toxoplasma gondii.* Mol Biochem Parasitol, 145: 125-7.
1102 106. Wan, K.L., V.B. Carruthers, L.D. Sibley, and J.W. Ajioka, 1997. *Molecular*
1103 *characterisation of an expressed sequence tag locus of Toxoplasma gondii encoding the*
1104 *micronemal protein MIC2.* Mol Biochem Parasitol, 84: 203-14.
1105 107. Garcia-Reguet, N., M. Lebrun, M.N. Fourmaux, O. Mercereau-Puijalon, T. Mann, C.J.
1106 Beckers, B. Samyn, J. Van Beeumen, D. Bout, and J.F. Dubremetz, 2000. *The microneme*

1107 *protein MIC3 of Toxoplasma gondii is a secretory adhesin that binds to both the surface*
1108 *of the host cells and the surface of the parasite.* Cell Microbiol, 2: 353-64.
1109 108. Brydges, S.D., X.W. Zhou, M.H. Huynh, J.M. Harper, J. Mital, K.D. Adjogble, W.
1110 Daubener, G.E. Ward, and V.B. Carruthers, 2006. *Targeted deletion of MIC5 enhances*
1111 *trimming proteolysis of Toxoplasma invasion proteins.* Eukaryot Cell, 5: 2174-83.
1112 109. Meissner, M., M. Reiss, N. Viebig, V.B. Carruthers, C. Toursel, S. Tomavo, J.W. Ajioka,
1113 and D. Soldati, 2002. *A family of transmembrane microneme proteins of Toxoplasma*
1114 *gondii contain EGF-like domains and function as escorters.* J Cell Sci, 115: 563-74.
1115 110. Hoff, E.F., S.H. Cook, G.D. Sherman, J.M. Harper, D.J. Ferguson, J.F. Dubremetz, and
1116 V.B. Carruthers, 2001. *Toxoplasma gondii: molecular cloning and characterization of a*
1117 *novel 18-kDa secretory antigen, TgMIC10.* Exp Parasitol, 97: 77-88.
1118 111. Harper, J.M., M.H. Huynh, I. Coppens, F. Parussini, S. Moreno, and V.B. Carruthers,
1119 2006. *A cleavable propeptide influences Toxoplasma infection by facilitating the*
1120 *trafficking and secretion of the TgMIC2-M2AP invasion complex.* Molecular Biology of
1121 the Cell, 17: 4551-4563.
1122 112. Carey, K.L., A.M. Jongco, K. Kim, and G.E. Ward, 2004. *The Toxoplasma gondii*
1123 *rhoptry protein ROP4 is secreted into the parasitophorous vacuole and becomes*
1124 *phosphorylated in infected cells.* Eukaryot Cell, 3: 1320-30.
1125 113. Cesbron-Delauw, M.F., B. Guy, G. Torpier, R.J. Pierce, G. Lenzen, J.Y. Cesbron, H.
1126 Charif, P. Lepage, F. Darcy, and J.P. Lecocq, 1989. *Molecular characterization of a 23-*
1127 *kilodalton major antigen secreted by Toxoplasma gondii.* Proc Natl Acad Sci U S A, 86:
1128 7537-41.
1129 114. Burg, J.L., D. Perelman, L.H. Kasper, P.L. Ware, and J.C. Boothroyd, 1988. *Molecular*
1130 *analysis of the gene encoding the major surface antigen of Toxoplasma gondii.* Journal of
1131 immunology, 141: 3584-91.
1132 115. Dubremetz, J.F., A. Achbarou, D. Bermudes, and K.A. Joiner, 1993. *Kinetics and pattern*
1133 *of organelle exocytosis during Toxoplasma gondii/host-cell interaction.* Parasitol Res,
1134 79: 402-8.
1135 116. Couvreur, G., A. Sadak, B. Fortier, and J.F. Dubremetz, 1988. *Surface antigens of*
1136 *Toxoplasma gondii.* Parasitology, 97 (Pt 1): 1-10.
1137 117. Sadak, A., Z. Taghy, B. Fortier, and J.F. Dubremetz, 1988. *Characterization of a Family*
1138 *of Rhoptry Proteins of Toxoplasma-Gondii.* Molecular and Biochemical Parasitology,
1139 29: 203-211.
1140 118. Morrissette, N.S. and L.D. Sibley, 2002. *Disruption of microtubules uncouples budding*
1141 *and nuclear division in Toxoplasma gondii.* J Cell Sci, 115: 1017-25.
1142 119. Jerka-Dziadosz, M., L.M. Jenkins, E.M. Nelsen, N.E. Williams, R. Jaeckel-Williams, and
1143 J. Frankel, 1995. *Cellular polarity in ciliates: persistence of global polarity in a*
1144 *disorganized mutant of Tetrahymena thermophila that disrupts cytoskeletal organization.*
1145 Dev Biol, 169: 644-61.
1146

1147 **Figure 1**

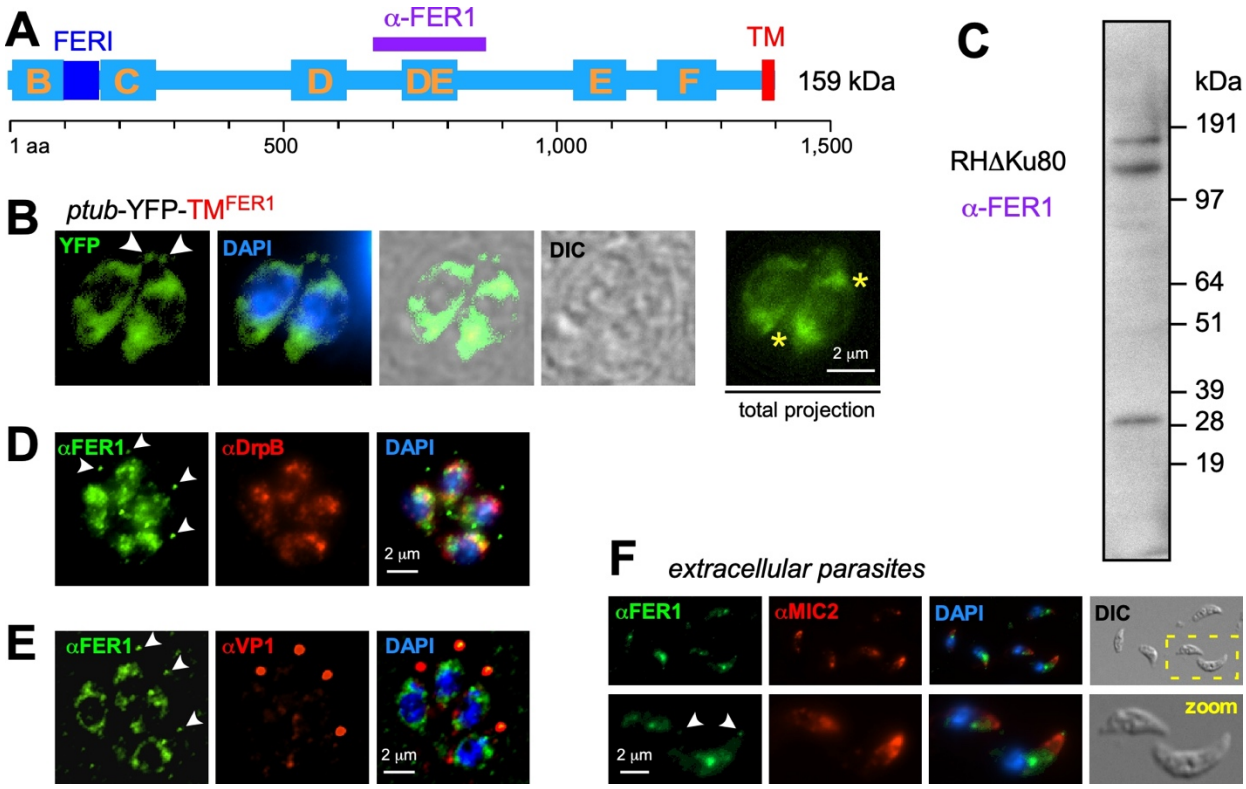

1148

1149 **Figure 1. FER1 localizes to the secretory pathway and the conoid region. A.** Schematic
1150 representation of TgFER1. Yellow letters mark the C2 domains; the aa 669-877 region used to
1151 generate a specific antiserum is marked in purple; FERI is a domain conserved in most ferlins
1152 with unknown function; TM is the transmembrane domain. **B.** Overexpression of a YFP fusion to
1153 the FER1 TM domain (C-terminal 31 aa, comprising 10 aa before the 21 extremely C-terminal
1154 TM domain) only under the tubulin promoter (*ptub*). Arrowheads mark YFP localization to the
1155 conoid region; yellow asterisk mark the perinuclear region reminiscent of the ER. Left panels
1156 represent a single z-layer from deconvolved images collected by wide-field microscopy; in the
1157 right panel all z-stacks are projected. **C.** Western blot analysis with the affinity purified guinea
1158 pig polyclonal antiserum generated against the FER1 region marked in panel A. Total lysate of
1159 wild type (RHΔKu80) parasites was loaded. **D-F.** Analysis of the affinity purified FER1
1160 antiserum by IFA co-stained with α-DrpB serum marking the ELC (D) and α-VP1 serum
1161 marking the plant like vacuole (E). Arrowheads mark FER1 localization to the conoid region,
1162 which colocalizes with VP1. The area corresponding with the yellow box in the top right panel
1163 of F is magnified in the lower panels (zoom). Parasites in A and F were fixed with 4% PFA,
1164 parasites in D and E with 100% methanol.

1165 **Figure 2**

1166

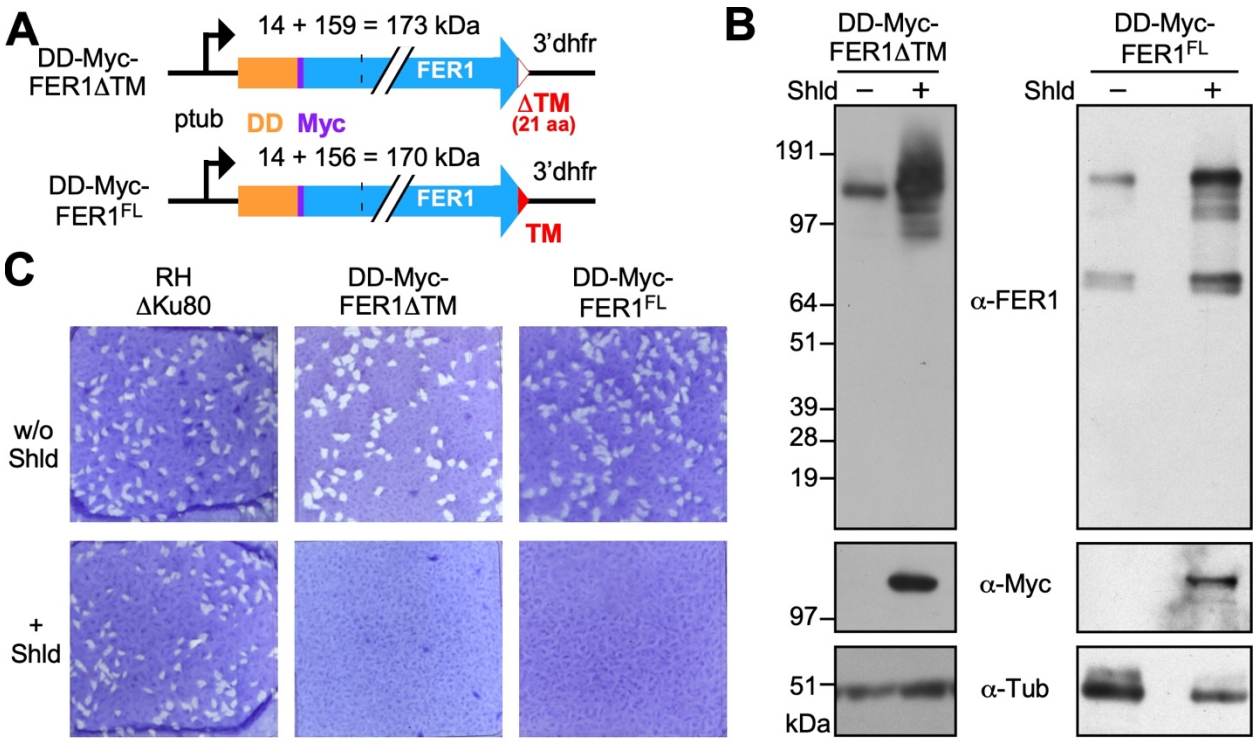

1167

1168

1169 **Figure 2. Generation and validation of conditional FER1 overexpression parasite lines. A.**
1170 Schematic representation of the overexpression constructs driven by the strong constitutive α-
1171 tubulin promoter (*ptub*). DD: destabilization domain; Myc: cMyc epitope tag; TM:
1172 transmembrane domain; FL: full length. **B.** Western blot analysis of the overexpression parasite
1173 lines. Polyclonal guinea pig FER1 antiserum as in Fig 1. Monoclonal antibody12G10
1174 recognizing α-tubulin was used as loading control. Parasites were induced with 1 µM Shield-1
1175 for 24 hrs. **C.** plaque assays of infected HFF monolayers grown for 7 days ± 1 µM Shield-1.

1176 **Figure 3**

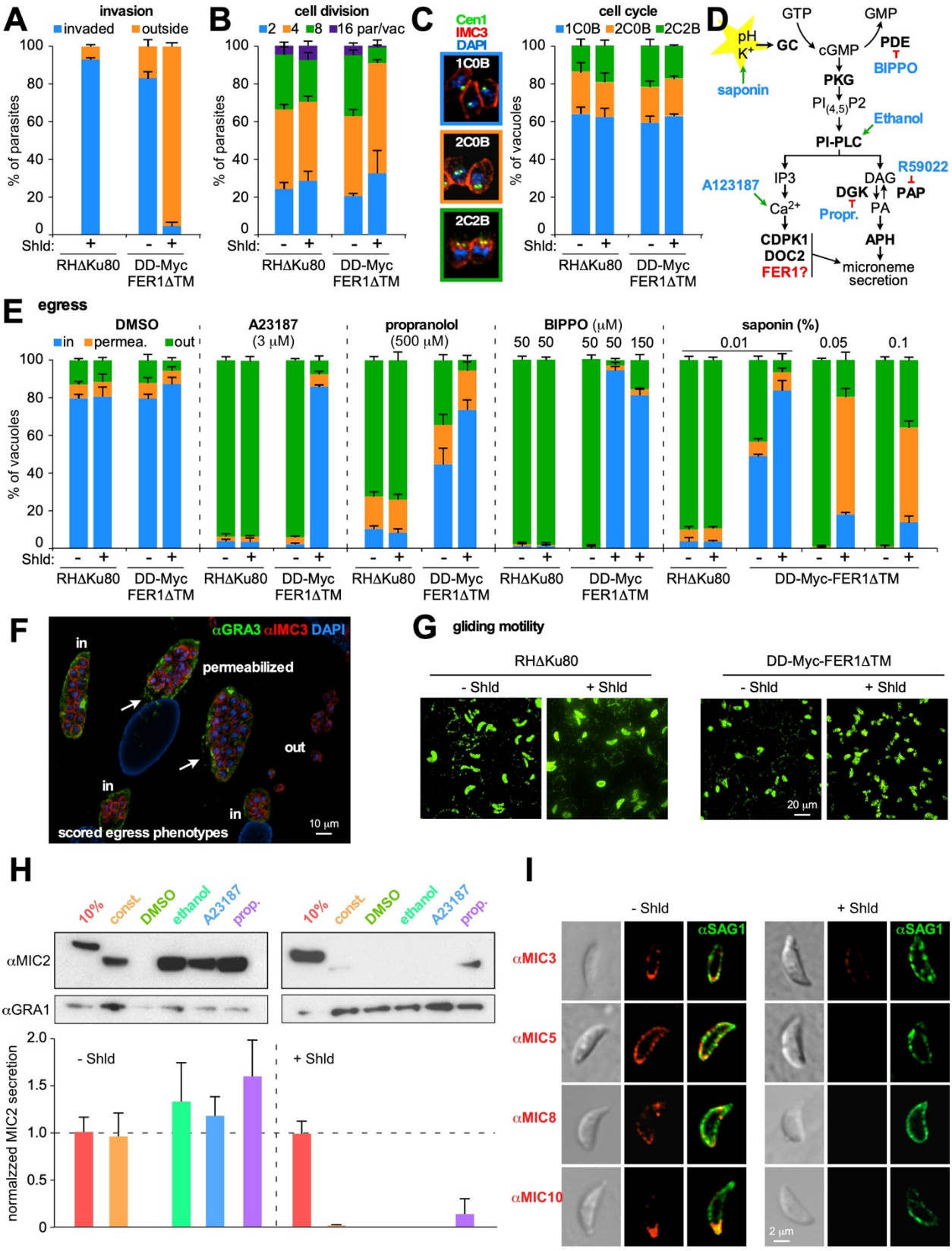

1177

1178

1179 **Figure 3. Phenotypic characterization of parasites overexpressing DD-Myc-FER1ΔTM. A.**
1180 Red-green invasion assay data reveal an invasion defect. **B, C.** Cell division and cell cycle
1181 progression analysis show that overexpression of DD-Myc-FER1ΔTM results in slightly slower
1182 reproduction rates (B), however a significant delay in cell cycle was not detected (C). Examples
1183 of the cell cycle stages quantified in the left of panel C are shown on the right. Parasites were
1184 allowed to invade for 2 hrs upon which 1 μM Shield-1 was added for 18 hrs. p=0.031 (*t*-test)
1185 accumulation of parasite in the 4-cells/vacuole stage. **D.** Schematic overview of signaling toward
1186 microneme secretion and egress, highlighting pharmacological agents acting on various events.
1187 **E, F.** Induced egress assays. Parasites grown for 30 hrs in fibroblasts and induced for 18 hrs with
1188 1 μM Shield-1 were triggered for egress with the pharmacologicals as indicated, fixed and
1189 stained with α-IMC3 (parasite cortex) and α-GRA3 (PVM) sera and scored for status of vacuole
1190 permeabilization and/or egress (F; representative image; arrows mark holes in the PVM of
1191 permeabilized vacuoles). n=3±std. Parasites were not under Shield-1 pressure during the 5 min
1192 pharmacological incubation. **G.** Trail assay using α-SAG1 serum to assess gliding motility
1193 capacity reveals that DD-Myc-FER1ΔTM parasites are unable to glide. Parasites were induced
1194 for 18 hrs ± 1 μM Shield-1, mechanically released from host cells and kept under 1 μM Shield-1
1195 throughout the 30 min gliding experiment at 37ºC. **H.** Assessment of microneme secretion by
1196 western blot detection of MIC2 released in the supernatant under various triggers. Parasites were
1197 induced 18 hrs with 1 μM Shield-1 and harvested by physical release from the host cell. 10%:
1198 10% of total lysate; const.: 1 hr constitutive secretion at 37ºC in absence of secretagogue; 1%
1199 ethanol; 2 μM A23187; 500 μM propranolol. DMSO is the vehicle control for A23187. Induced
1200 secretion for 5 min at 37ºC. Bottom of panel represents quantified secretion normalized to the
1201 GRA1 signal and to the 10% loading control for each condition. n=3±std. Parent line controls in
1202 Supplementary Fig S1. Parasites were not under Shield-1 pressure during secretion assay. **I.**
1203 Secretion of the Rab5/A-dependent microneme population was assessed by IFA on non-
1204 permeabilized parasites induced for 18 hrs ± 1 μM Shield-1, mechanically released, and exposed
1205 to fresh host cells for 5 min at 37ºC. Parasites were not under Shield-1 pressure during assay.

1206 **Figure 4**

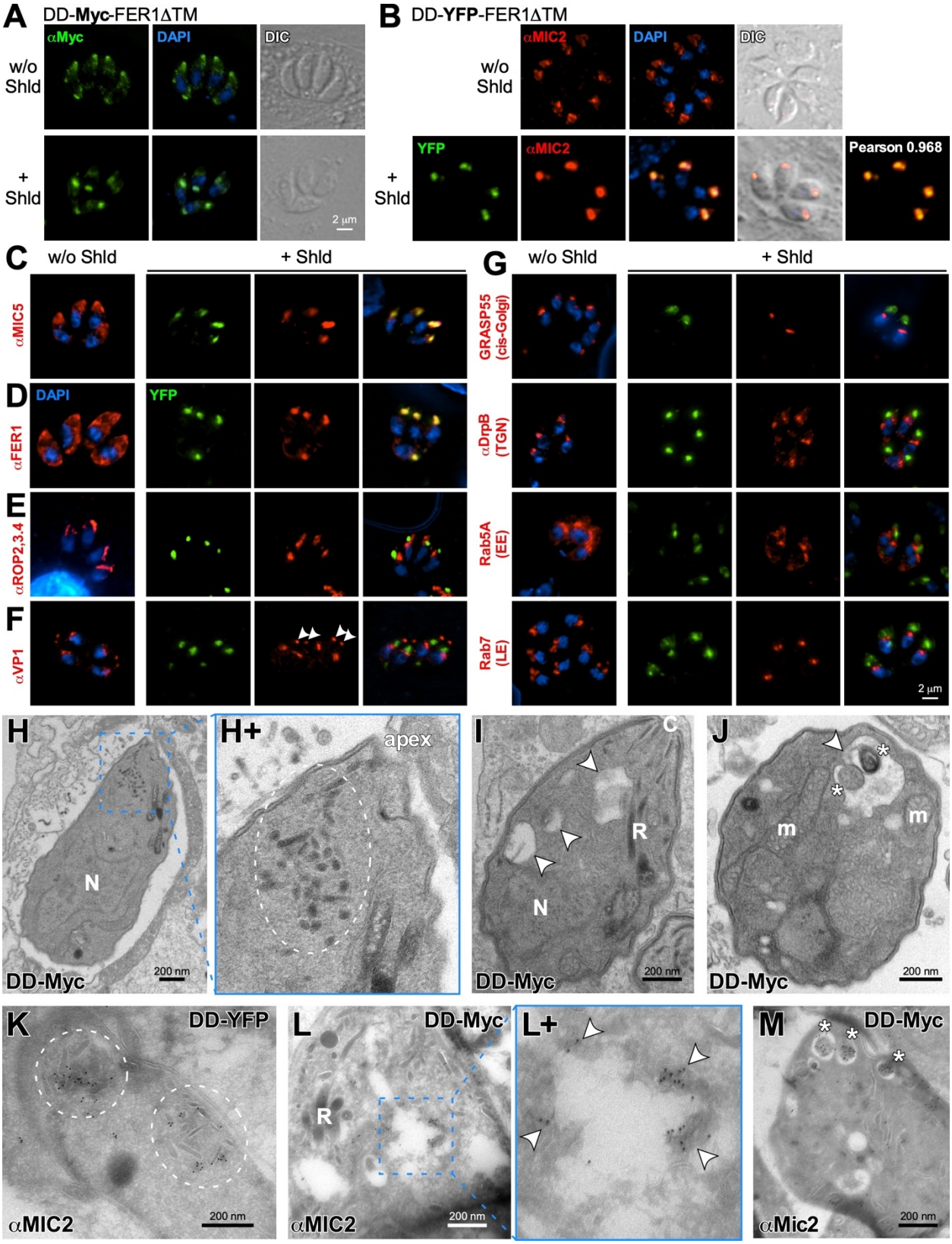

1207

1208 **Fig 4. Overexpression of dominant negative FER1ΔTM constructs result in microneme**
1209 **mislocalization. A, B.** Overexpression of DD-**Myc**-FER1ΔTM (A) or DD-**YFP**-FER1ΔTM (B)
1210 leads to accumulation of microneme protein, visualized with α-MIC2, in a central, apical
1211 location. YFP and MIC2 co-localization was assesses by Pearson correlation. **C.** Microneme
1212 proteins of the Rab5A/C-dependent trafficking pathway, visualized with α-MIC5, also
1213 accumulate in the FER1 compartment. **D.** α-FER1 serum confirms exclusive accumulation in the
1214 microneme protein compartment. **E.** ROP proteins do not accumulate and rhoptry morphology is
1215 normal. **F.** Co-localization of VP1 and the YFP accumulation is not detected. Note the apical
1216 VP1 localization is still present (arrowheads). **G.** Markers for cis Golgi, trans-Golgi network
1217 (TGN) as well as early (EE) and late (LE) endosome markers localize normally and do no co-
1218 localize with the YFP accumulation. In all IFA experiments parasites were treated with 1 μM
1219 Shield-1 for 18 hrs; results with additional independent markers for the same compartments are
1220 provided in Supplementary Fig S2. **H-J.** TEM of DD-Myc-FER1ΔTM overexpressing parasites
1221 induced for 16 hrs with 1 μM Shield-1. N, nucleus; R, rhoptries; m, mitochondrion. Dotted circle
1222 marks atypical accumulation of microneme organelles in the apical end. Arrowheads mark
1223 enlarged vacuoles, sometimes with *-marked accumulations inside. **K-M.** IEM with MIC2
1224 antibody (10 nm gold particles) of DD-Myc-FER1ΔTM or of DD-YFP-FER1ΔTM
1225 overexpressing parasites induced for either 7 hrs with 3 μM Shield-1 (K,M) or 16 hrs with 1 μM
1226 Shield-1 (L). Dotted circles mark atypical microneme accumulations in the cytosol. R, rhoptries.
1227 Arrowheads mark MIC2 signal at the edge of an enlarged vacuole. Asterisks mark accumulations
1228 inside vacuoles containing MIC2 protein.

1229 **Figure 5**

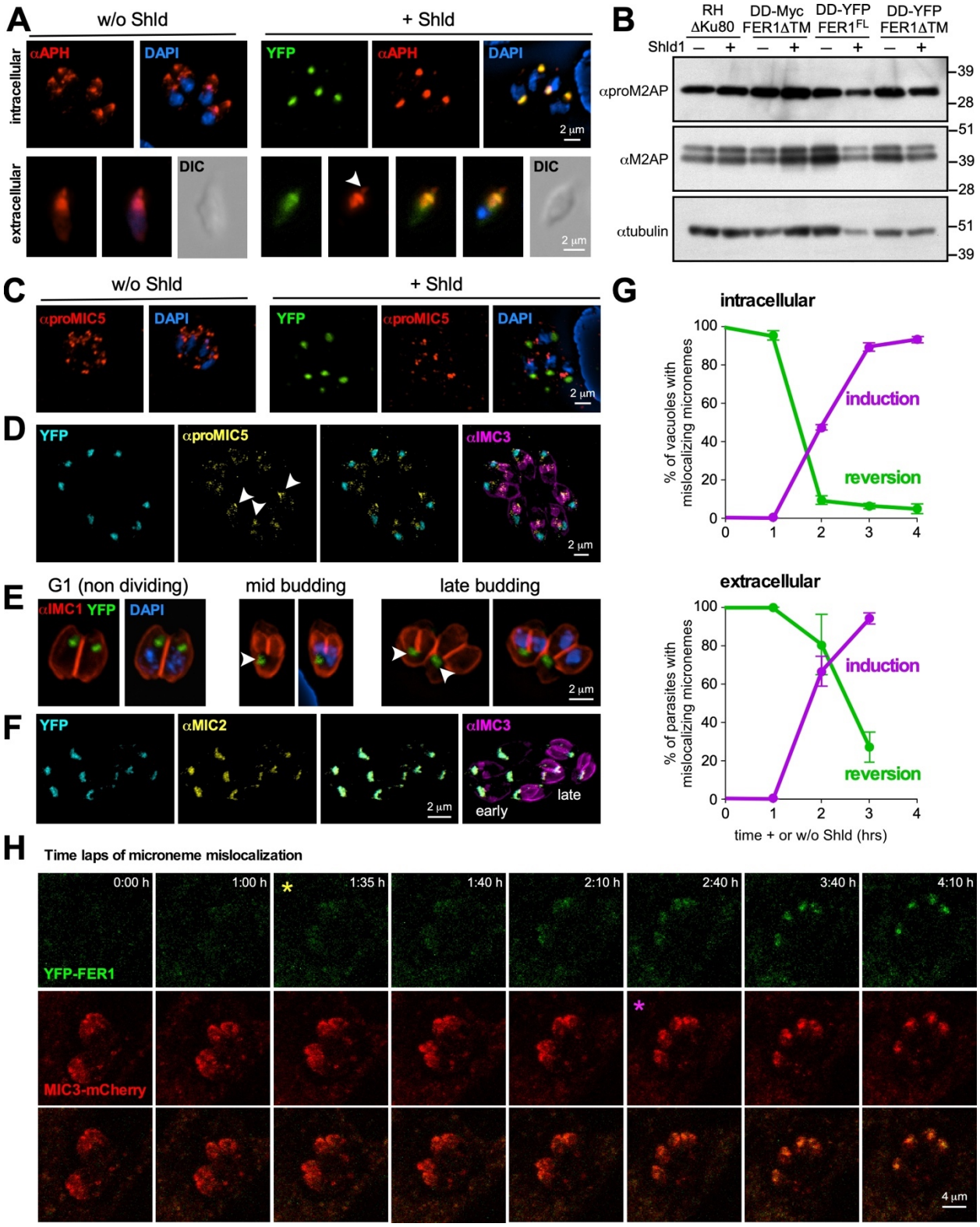

1230

1231

1232 **Figure 5. Microneme trafficking dynamics upon DD-YFP-FER1ΔTM overexpression.** In all
1233 IFA experiments parasites were treated with 1 μM Shield-1 for 18 hrs. **A.** Mislocalized
1234 micronemes are coated with the mature microneme marker APH in both intracellular (top) and
1235 extracellular (bottom) parasites. Arrowhead marks APH signal in the conoid where YFP signal is
1236 absent. **B.** Normal maturation by pro-peptide processing in the ELC-PLV compartment of
1237 microneme proteins in induced and various control parasites as indicated was demonstrated by
1238 western blot using antiserum against the pro-peptide of M2AP (α-proM2AP) and antiserum
1239 against the mature section of the protein (α-M2AP). α-tubulin serves as loading control. **C.** IFA
1240 with α-proMIC5 revealed that microneme accumulation is not due to arrested trafficking since
1241 proMIC5 is only observed in the ELC-PLV compartment in newly forming daughter buds. **D.**
1242 Induced mutants co-stained with YFP, proMIC5, and IMC3 antiserum to track the timing and
1243 localization of proMIC5 processed as indicated. Arrowheads mark the proMIC5 compartment
1244 within budding daughter buds. Note that DD-YFP-FER1ΔTM is exclusively present in the
1245 mother parasites and does not localize to the budding daughters**. E.** Induced mutants co-stained
1246 with IMC1 antiserum to track division stages as indicated. Arrowheads mark the mother
1247 parasite's YFP accumulation migrating into a basal direction during progression of daughter
1248 budding. Note the absence of YFP in the daughter buds.
1249 **F.** Induced mutants co-stained with YFP, MIC2, and IMC3 antisera to track the localization of
1250 mature MIC2 protein through cell division. Note the consistent colocalization of DD-YFP-
1251 FER1ΔTM with MIC2 throughout the division stages, indicating that the daughter buds never
1252 assemble mature micronemes. **G.** Time courses of the incidence of vacuoles or individual
1253 parasites with mislocalizing micronemes in intracellular and extracellular parasites, respectively,
1254 visualized through α-MIC2 IFA. At least 100 vacuoles or parasites were counted per time point.
1255 n=3±std. In reversion experiments, intracellular parasites were induced for 18 hrs with Shield-1.
1256 **H.** Select panels from time lapse experiment with DD-YFP-FER1ΔTM parasites co-transfected
1257 with MIC3-mCherry to track microneme localization dynamics. At t=0, 2 μM Shield-1 was
1258 added. The first time point at which the piling up of YFP-FER1 could be convincingly observed
1259 is marked with a yellow asterisk; the first time where MIC3-mCherry can be seen re-localizing
1260 from the apical cortex to the central apical localization co-localizing with YFP-FER1 is marked
1261 with a purple asterisk. Panels from supplementary movie S1.

1262 **Figure 6**

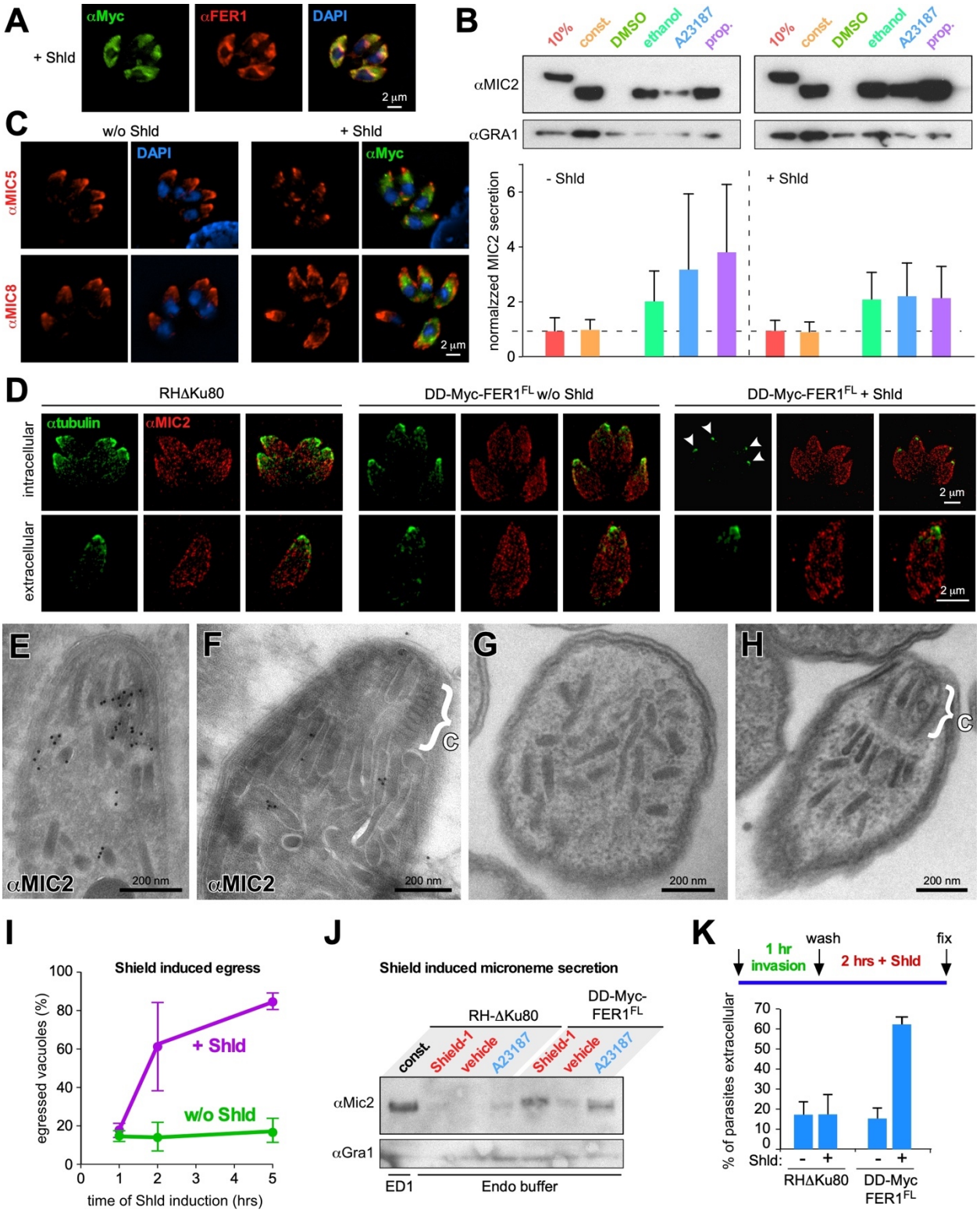

1263

1264

1265

1266 **Figure 6. DD-Myc-FER1^{FL} overexpression results in apical microneme migration and a**
1267 **burst of signaling-independent microneme release. A.** Co-staining of α-Myc and α-FER1 sera
1268 by IFA shows that overexpressed DD-Myc-FER1^{FL} localizes to the cytoplasm. Total projection
1269 of deconvolved image is shown. **B.** Assessment of microneme secretion by western blot through
1270 MIC2 release in the supernatant under various triggers. Parasites were induced 6 hrs with 1 μM
1271 Shield-1 and harvested by physical release from the host cell. 10%: 10% of total lysate; const.: 1
1272 hr constitutive secretion at 37ºC in absence of secretagogue; 1% ethanol; 2 μM A23187; 500 μM
1273 propranolol. DMSO is the vehicle control for A23187. Induced secretion for 5 min at 37ºC.
1274 Bottom of panel represents quantified secretion normalized to the GRA1 signal and to the 10%
1275 loading control for each condition. n=3±std. Parent line controls in Supplementary Fig S1.
1276 **C.** Immunofluorescence of DD-Myc-FER1^{FL} co-stained with α-MIC5 and α-MIC8 and α-FER1
1277 shows that this Rab5A/C-dependent microneme population becomes scattered upon phenotype
1278 induction, although an extreme apical focal point remains. **D.** Super-resolution SIM microscopy
1279 of wild-type and DD-Myc-FER1^{FL} co-stained with α-MIC2 and α-Tgβ-tubulin further details
1280 apical microneme translocation in intracellular parasites upon Shield-1 induction (arrowheads).
1281 In extracellular parasites an increased apical accumulation of micronemes is seen across control
1282 and mutant parasites regardless of phenotype induction. **E, F.** IEM of DD-Myc-FER1^{FL}
1283 overexpressing parasites stained with MIC2 antibody (10 nm gold particles) induced for 16 hrs
1284 with 1 μM Shield-1. MIC signal localizes to apically accumulated micronemes which display a
1285 stretched or extended morphology. Accolade bracket marks conoid (c). **G, H.** TEM of
1286 extracellular DD-Myc-FER1^{FL} overexpressing parasites induced for 3 hrs with 2 μM Shield-1.
1287 Cross section in J shows the extended feature or the densely packed microneme organelles,
1288 whereas K shows the radial micronemes just below the conoid, again with a slightly stretched or
1289 extended appearance. Accolade bracket marks conoid (c). **I.** Time course of Shield-1 Induced
1290 egress. Parasites grown for 30 hrs in fibroblasts and induced for 1 μM Shield-1 for the times as
1291 indicated, fixed with 100% methanol and stained with α-Myc, α-MIC8 and DAPI. Intact
1292 vacuoles per field were scored as proxy for egress. n=3±std. **J.** Shield-1 induced microneme
1293 secretion in Endo buffer. Western blot of MIC2 release in the supernatant; GRA1 as control.
1294 Const.: Constitutive 1 hr at 37ºC in standard ED1 culture medium. In intracellular conditions
1295 mimicking Endo buffer, parasites were induced with 1 μM Shield-1 for 2 hrs at 37ºC; vehicle
1296 represent the solvent of the Shield-1 stock (0.1% ethanol end concentration). A23187 (1 μM)

1297 was added for 5 min in the end of the 2 hr window and is additive to the constitutive secretion.
1298 **K.** Modified red-green invasion assay followed by Shield-1 induction. Top schematic shows
1299 parasites were allowed to invade for 1 hr min at 37ºC followed by a wash to remove non-invaded
1300 parasites and 2 hrs 1 μM Shield-1 induction followed by the red-green invasion assay. Lower
1301 panel shows the relative number of parasites observed outside the host cell, indicating
1302 overexpression of FER1 leads to microneme secretion, egress, and host cell destruction. n=4±std.

1303 **Figure 7 - FER1 is Ca^{2+}dependendent**

1304

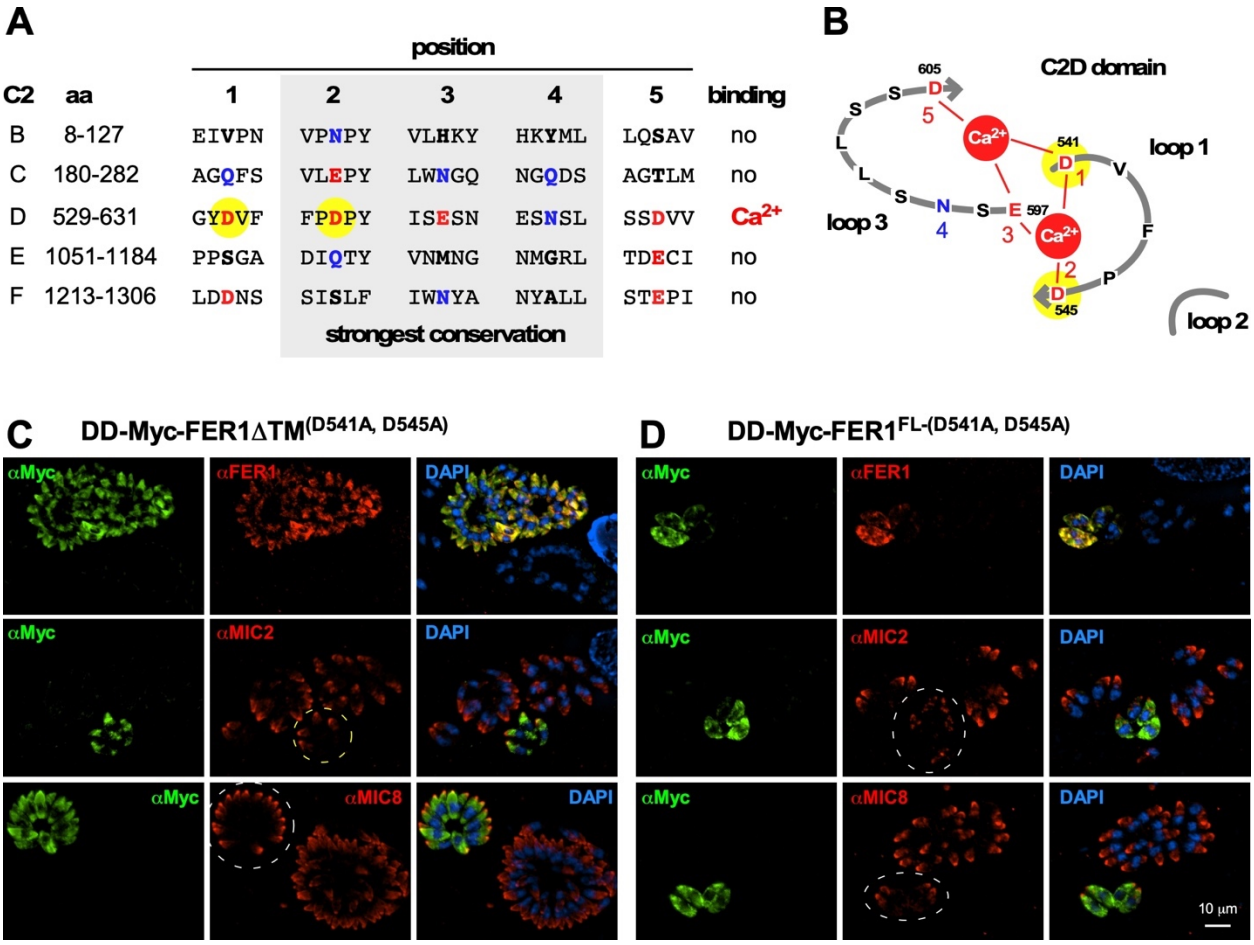

1305

1306

1307 **Figure 7. FER1-mediated trafficking of micronemes relies on predicted Ca^{2+}-binding**
1308 **residues. A.** Sequence analysis of the five conserved key positions (#1-5) in the C2A-F domain
1309 loops interfacing with Ca^{2+} [104]. D or E residues (red) stabilize Ca^{2+}, N or Q (bleu) are expected
1310 to support phospholipid binding. Positions 2, 3, and 4 shaded in grey are more strongly
1311 conserved than positions 1 and 5. Yellow highlighted residues were mutated to A to abolish the
1312 predicted Ca^{2+}-binding capacity in the C2D domain resulting in the mutant FER1$^{(DD541,545AA)}$
1313 allele. **B.** Models of the C2D domain loops and putative Ca^{2+} binding capacity. Yellow
1314 highlighted residues as in panel A. **C, D.** Transient overexpression DD-Myc-
1315 FER1ΔTM$^{(D541A,D545A)}$ DD-Myc-FER1$^{FL-(D541A,D545A)}$, respectively, co-stained for Myc, FER1,
1316 MIC2 and MIC8, as indicated. Each panel contains transfected (Myc positive) and non-
1317 transfected (Myc negative) parasite examples. Note that due to the high level of overexpression

1318 the FER1 signal in non-transfected parasites is below the detection limit under these conditions.
1319 Following electroporation, parasites were allowed to invade for 2 hrs before 1 μM Shield-1
1320 induction for 24 hrs. Yellow dotted circle marks normal MIC morphology while white dotted
1321 circles mark aberrant MIC morphology in vacuoles overexpressing the D541A,545A FER1
1322 alleles as indicated.

1323 **Figure 8**

1324

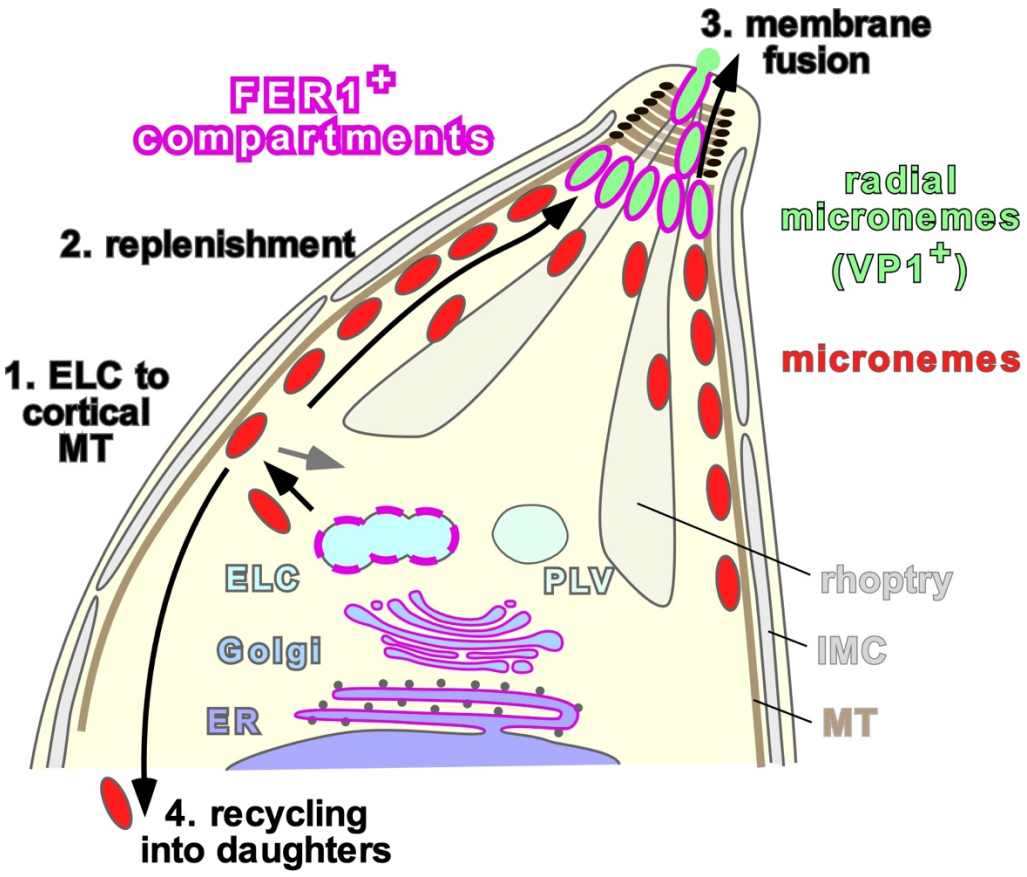

1325

1326

1327 **Figure 8. Working model of FER1 mediated microneme events.** FER1 mediates the following
1328 trafficking steps: 1. From the ELC to the subpellicular microtubules (actin dependent); 2.
1329 microneme migration along the subpellicular microtubules; 3. Microneme membrane fusion with
1330 the plasma membrane; 4. Recycling of micronemes into the budding daughters (actin dependent).
1331 We hypothesize the radial micronemes represent a readily releasable vesicle pool primed for
1332 secretion by VP1-mediated acidification. MT: microtubules; ELC: endosome-like compartment;
1333 PLV: plant like vacuole or VAC.

1334 **Supplementary data**

1335

1336 **Supplementary Movie S1.** Time lapse experiment of DD-YFP-FER1ΔTM parasites co-
1337 transfected with MIC3-mCherry to track the micronemes. At t=0, 2 µM Shield-1 was added and
1338 images collected every 5 minutes. Scale bars 80 µm.

1339

1340 **Supplementary movie S2.** Time lapse experiment of DD-YFP-FER1ΔTM parasites co-
1341 transfected with IMC3-mCherry to track cell division status. At t=0, 2 µM Shield-1 was added
1342 and images collected every 5 minutes. Scale bars 80 µm.

1343

1344

1345 **Supplementary Figure S1**

1346

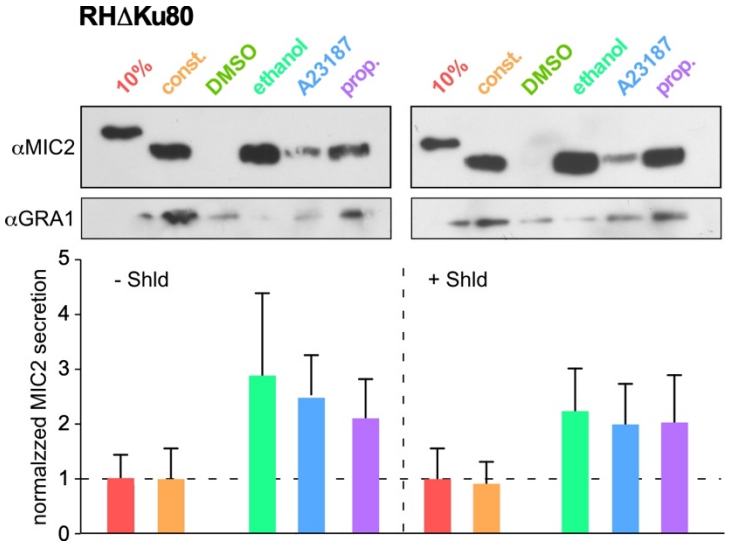

1347
1348

1349 **Supplementary Figure S1. Microneme secretion assessment of the RHΔKu80 parent line**
1350 **control.** Assessment of microneme secretion by western blotting by detecting MIC2 release in
1351 the supernatant under various triggers. Parasites were induced 18 hrs with 1 µM Shield-1 and
1352 harvested by physical release from the host cell. 10%: 10% of total lysate; const.: 1 hr
1353 constitutive secretion at 37ºC in absence of secretagogue; 1% ethanol; 2 µM A23187; 500 µM
1354 propranolol. DMSO is the vehicle control for A23187. Induced secretion for 5 min at 37ºC.
1355 Bottom of panel represents quantified secretion normalized to the GRA1 signal and to the 10%
1356 loading control for each condition. n=3±std.

1357 **Supplementary Figure S2**

1358

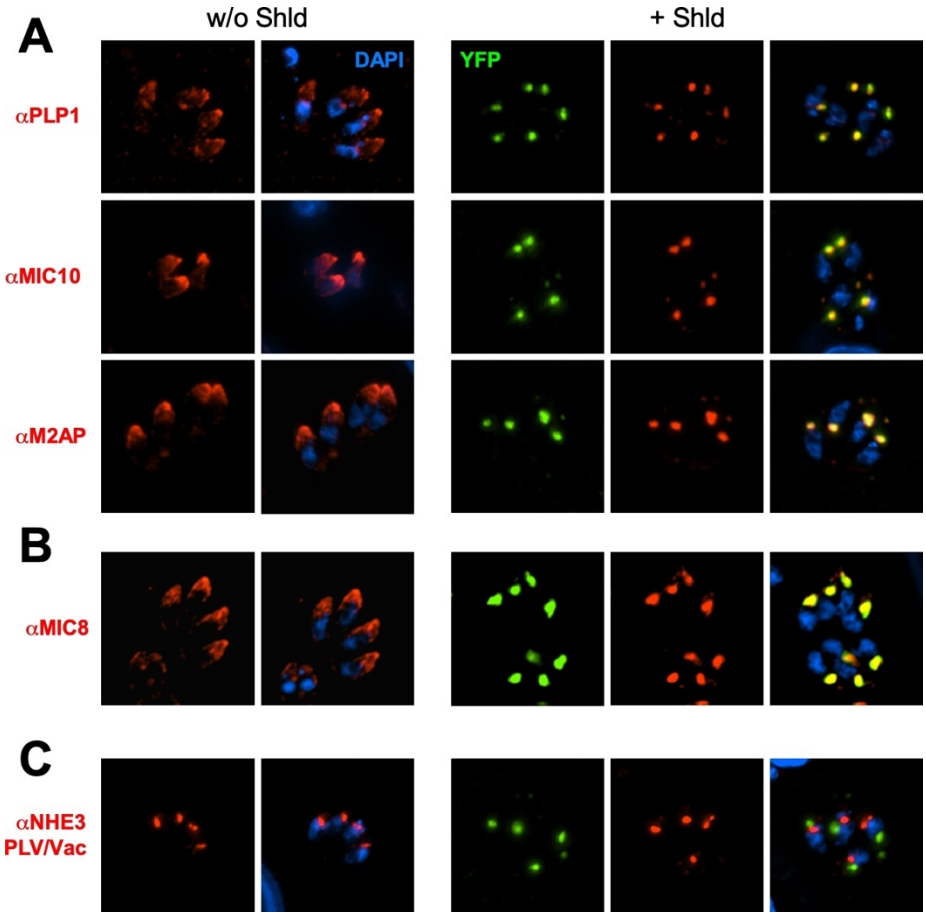

1359

1360

1361 **Supplementary Figure S2.** Additional localization data in the DD-YFP-FER1 Δ TM dominant

1362 negative mutant. **A.** Additional microneme proteins in the MIC2 group. **B.** Additional protein in

1363 the MIC3/5/8 group. **C.** NHE3 is a specific marker of the PLV compartment. Parasites were

1364 treated with 1 μM Shield-1 for 18 hrs.

1365 **Supplementary Figure S3**

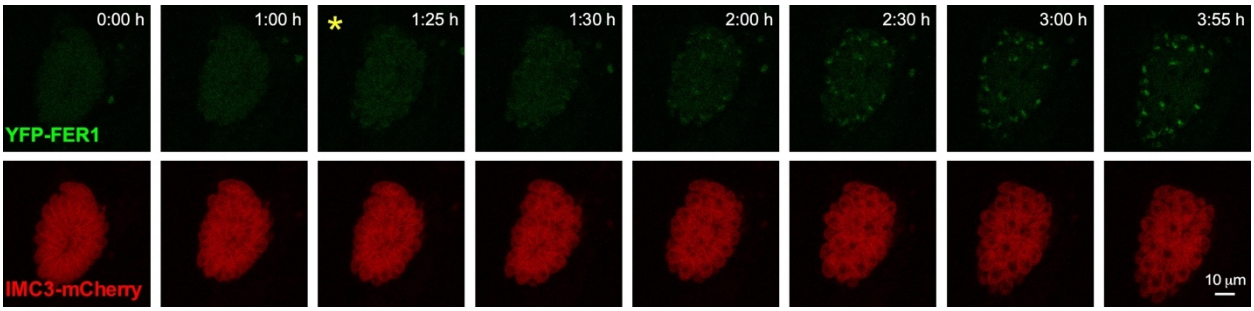

1366

1367 **Supplementary Figure S3.** Select panels from time lapse experiment of DD-YFP-FER1ΔTM
1368 parasites co-transfected with IMC3-mCherry to track cell division. At t=0, 2 µM Shield-1 was
1369 added. The first time point at which the piling up of YFP could be convincingly observed is
1370 marked with a yellow asterisk. Panels from supplementary movie S2.

1371 **Supplementary Table S1.** Description of oligonucleotides used. Restriction enzyme sites
1372 underlined.
1373
1374 *Cloning of tub-YFP-TM(FER1)*
1375 4786 FER1-TM-F(Gib) GCATGGACGAGCTGTACAAGCCTAGGAGCGCCATTATGAGTGGGCTG
1376 4788 3'dhfr-Not-R(Gib) CGAATTGGAGCTCCACCGCGGTGGCGGCCGC
1377
1378 *Cloning of tub-DD-YFP-FER1^{FL}/sagCAT*
1379 1573 YFP-109420_F GGTCCCCTAGGATGGCGGCGAAGGCGATC
1380 1574 YFP-109420_R GGTCCCCCGGGTTATTTGAGGAGAAACATAACAAAGATGACTAGCGC
1381 1635 5xTy_F(avrII) GGACCCCTAGGGAGGTCCATACTAACCAGGATCCACTTGACGGCGAGG
1382 1636 DD_R(MfeI-EcoRV) GGACCGATATCTTACAATTGTTCCAGTTTTAGAAGCTCCACACGG
1383
1384 *Internal primers used to for FER1 CDS Sanger sequencing*
1385 2717 Fer1-RACE-F CGCACCAACGAGAGGCGCTCGCAGCTA
1386 2748 FER1_SeqF2 ATGCGTTCCCTGTTTCGAT
1387 2749 FER1_SeqF3 GTACAGCCTCCGCTCTCTTG
1388 2750 FER1_SeqF4 TGTCTGTGTCTCTCCCCAAA
1389
1390 *Cloning of tub-DD-YFP-FER1ΔTM/sagCAT*
1391 1651 FLPnoTM(NheI)_F GGTCCGCTAGCCCTGAAGAGGAAACCTACG
1392 1652 FLPnoTM(XmaI)_R GGTCCCCCGGGTTACGTCCATTTCAGCCCACTCATAATGGC
1393
1394 *Site Directed Mutagenesis of C2D*
1395 4833 SDM-FER1-1-2-F TCCGGCTCCCTACATCCAAGTGGAACTG
1396 4834 SDM-FER1-1-2-R AACACGGCGTAGCCGACAGCTGGGAG
1397
1398 *6His-FER1 for antiserum generation*
1399 2787 Ava-LIC-Fer1-F GGGTCCTGGTTCGATGTCGACGAAGGAAGGCAACATTC
1400 2903 Ava-LIC-Fer1-R CTTGTTCGTGCTGTTTATTAGAGTTGCTCAGGCGTGAAGC
1401
1402 *Cloning of pmic3-MIC3-Cherry-DHFR*
1403 4864 gibpMIC3-MIC3-F GGAGATGACGAGACGTTTAAACGAGGAAAGTGGGGGGGGGGG
1404 4865 gibpMIC3-MIC3-R GTTATCCTCCTCGCCCTTGCTCACCCTAGGGAGACTCGCTGGGTACCTTCGTC

1405 **Supplementary Table S2. Description of plasmids used.**

1406

Plasmid	Source and reference
ptub-DD-YFP-FER1ΔTM/sagCAT	In house [this paper]
ptub-DD-Myc-FER1ΔTM/sagCAT	In house [this paper]
ptub-DD-Myc-FER1ΔTM(^{D541A,D545A})/sagCAT	In house [this paper]
ptub-DD-Myc-FER1^{FL}/sagCAT	In house [this paper]
ptub-DD-Myc-FER1$^{FL\ (D541A,D545A)}$/sagCAT	In house [this paper]
ptub-YFP-TM^{FER1}/sagCAT	In house [this paper]
ptub-IMC3-mCherryRFP/sagCAT	In house [95]
pmic3-MIC3-mCherryRFP/hxgprtDHFR	In house [this paper]
ptub-GRASP55-RFP/sagCAT	Graham Warren [105]
Rab5A-HA OE Transient overexpression	Sabrina Marion [23]
Rab7-HA OE Transient overexpression	Sabrina Marion [23]

1407

1408 **Supplementary Table S3. Description of antibody and antisera used.**

1409

Name (monoclonal)	Species	Dilution (IFA)	Dilution (western)	Source and reference
cMyc (9E10)	mouse	1:50	1:50	Santa Cruz Biotech
HA (3F10)	mouse	1:3000		Roche
MIC2 (6D10)	mouse	1:2000	1:8000	David Sibley [106]
MIC2	rabbit	1:1000	1:8000	David Sibley [106]
MIC3	rabbit	1:100	1:400	Jean-François Dubremetz [107]
MIC5	rabbit	1:500	1:10000	Vern Carruthers [108]
MIC8	rabbit	1:1000		Dominique Soldati [109]
MIC10	rabbit	1:500	1:15000	Vern Carruthers [110]
M2AP	rabbit	1:1000	1:1000	Vern Carruthers [111]
proM2AP	rabbit	1:1000	1:1000	Vern Carruthers [111]
proMIC5	rabbit	1:500		Vern Carruthers [60]
proROP4	rabbit	1:750		Gary Ward [112]
GRA1 (TG17.43)	mouse	1:500	1:15000	BioVision.com [113]
SAG1 (DG52)	mouse	1:500		Jeroen Saeij [114]
GRA3 (T62ch)	mouse	1:500		Maryse Lebrun, Jean-François Dubremetz [115]
SAG1 (T41E5)	mouse & rabbit	1:500		Jean-François Dubremetz [116]
ROP2,3,4	mouse	1:250		Maryse Lebrun [117]
DrpB	rat	1:2000		Peter Bradley [50]
VP1	rabbit	1:4000		Silvia Moreno [51]
APH	rabbit	1:1000		Dominique Soldati [28]
IMC3	rat	1:2000	1:1000	[95]
hCentrin	rabbit	1:1000		Iain Cheeseman, unpublished
Tg-β-tubulin	rabbit	1:500		Naomi Morrissette [118]
α-tubulin (12G10)	mouse	1:2000	1:100	Developmental Studies Hybridoma Bank [119]
NHE3	guinea pig	1:1500		Gustavo Arrizabalaga [54]
FER1	guinea pig	1:1000	1:1000	This paper

1410